A Facile Synthesis of Binary CuO/TiO_2 Heterojunction in Glass Matrix as a Photocatalyst for Dye Degradation.

Dissertation submitted to

Visvesvaraya National Institute of Technology, Nagpur

In partial fulfillment of the requirements for the award of

the degree

Masters of Science

In

Physics

by

Abhilasha Kumari (MS23PHY022)

under the guidance of

Dr. R.S. Gedam

Department of Physics

Visvesvaraya National Institute of Technology

Nagpur 440010 (India)

2023-25

A Facile Synthesis of Binary CuO/TiO_2 Heterojunction in Glass Matrix as a Photocatalyst for Dye Degradation.

Dissertation submitted to

Visvesvaraya National Institute of Technology, Nagpur

In partial fulfillment of the requirements for the award of

the degree

Masters of Science

In

Physics

by

Abhilasha Kumari (MS23PHY022)

under the guidance of

Dr. R.S. Gedam

Department of Physics

Visvesvaraya National Institute of Technology

Nagpur 440010 (India)

2023-25

©Visvesvaraya National Institute of Technology(VNIT) 2009

Department of Physics

Visvesvaraya National Institute of Technology, Nagpur

Dissertation Approval Sheet

Dissertation entitled **—A Facile Synthesis of Binary CuO/TiO_2 Heterojunction in Glass Matrix as a Photocatalyst for Dye Degradation,** by Abhilasha Kumari is approved for the degree of Master of Science in Physics**.**

(Name:) **(Name:)**

Supervisor **External Examiner**

(Name:)

Chairman

Date:

Place

Department of Physics

Visvesvaraya National Institute of Technology, Nagpur

Declaration

I, Abhilasha Kumari, hereby declare that this dissertation titled **"A Facile Synthesis of Binary CuO/TiO_2 Heterojunction in Glass Matrix as a Photocatalyst for Dye Degradation"** was carried out by me in the Department of Physics of Visvesvaraya National Institute of Technology, Nagpur. The work is original and has not been submitted earlier, whole or in part, for the award of any degree/diploma at this or any other Institution / University.

Abhilasha Kumari

Date:

Certificate

This is to certify that the dissertation titled **"A Facile Synthesis of Binary CuO/TiO_2 Heterojunction in Glass Matrix as a Photocatalyst for Dye Degradation"** is submitted by **Abhilasha Kumari** in partial fulfillment of the requirements for the award of the degree of **Master of Science in Physics**, VNIT Nagpur. The work is comprehensive, complete, and fit for final evaluation.

Supervisor,
Dr. R. S. Gedam
Professor
Dept. of Physics, VNIT, Nagpur

HOD

Department of Physics

VNIT, Nagpur

Date:

Visvesvaraya National Institute of Technology, Nagpur

Non-Plagiarism Certificate

Certified that M.Sc. Dissertation titled "**A Facile Synthesis of Binary CuO/TiO_2 Heterojunction in Glass Matrix as a Photocatalyst for Dye Degradation**" submitted by Abhilasha Kumari, Enrolment number MS23PHY022 ID no. 30707, is original in nature and not copied from any literature material.

ORIGINALITY REPORT

22%	14%	16%	8%
SIMILARITY INDEX	INTERNET SOURCES	PUBLICATIONS	STUDENT PAPERS

Abhilasha Kumari
(MS23PHY022)
ID No.- 30707

Dr. R.S. Gedam
Professor
Department of Physics
VNIT,Nagpur

ACKNOWLEDGMENT

At the beginning of this thesis, I would like to express my honest and heartfelt gratitude to all of the individuals who have supported me in this journey. I would not have progressed in my project without their active direction, assistance, cooperation, and encouragement.

Firstly, I would like to offer my sincere gratitude to my thesis supervisor, **Prof. R. S. Gedam, Department of Physics, VNIT, Nagpur (Maharashtra)**. His patience, excitement, cooperation, and advice inspired me to deliver this research effort in its current shape. His excellent, precise guidance enriched this work well beyond my expectations. I am also grateful for his constant advice, helping nature, and elderly support, which made a significant difference in my life.

I am extremely thankful and pay my special honor to Miss Ashwini S. Gadge for their endless support and dedicated assistance.

I would like to thank Miss. Yogita Shendre for their motivation and sound guidance.

I would be remiss in not mentioning my parents and the whole family, who always encourage me emotionally and financially. They always give me inspiration and hope for doing great in life.

Lastly, I would like to mention my dear friends and classmates for their cooperation, I am gratefully indebted for their valuable support and understanding.

(Abhilasha Kumari)

ABSTRACT

In the present project work, SiO_2-B_2O_3-Na_2O-K_2O-Al_2O_3 (sodium borosilicate glass), with CuO of 2 wt% and TiO_2 of 1 wt%, was synthesized using the conventional melt quench method. The present project work is focused on the photocatalytic activity of CuO/TiO_2 Quantum dots for indigo carmine dye degradation. Growth of CuO/TiO_2 was done by an optimized single-step heat-treatment schedule. The characterizations of synthesized QDs were carried out by DTA, XRD, Raman, FTIR, SEM & EDS, HRTEM, UV-Vis, and Photoluminescence study. The XRD confirmed the amorphous structure of glass. Raman analysis revealed the formation of the crystalline anatase and brookite phases of TiO_2 after heat treatment to grow CuO/TiO_2 QDs. The surface morphology and existence of elements in the prepared samples were analysed by the SEM and EDS analysis. HRTEM was employed to examine the shape and size of quantum dots (QDs) embedded in the glass matrix and found to be 2.40 nm. The shifting of the absorption edge toward the visible region and the separation of photogenerated charge carriers were analyzed by UV-Vis and photoluminescence spectra, respectively. The prepared sample was tested for photocatalytic performance against IC dye degradation, and the composition with the lowest PL intensity shows the degradation efficiency (92.52%) within 5hr under sunlight irradiation.

LIST OF FIGURES

FIGURE NO.	PARTICULARS	PAGE NO.
1.1	Electron-Hole production	5
1.2	Mechanism of photocatalysis	6
1.3	Variation of energy level with dimension	8
1.4	Crystalline and amorphous structures	10
1.5	Components of glass	11
1.6	Volume vs Temperature graph of glass formation	12
3.1	Synthesis of CuO/TiO_2 quantum dots by Melt Quench Method	18
3.2	Schematic diagram of differential thermal analysis	20
3.3	DTA curve	20
3.4	STAT7200 HITACHI	21
3.5	X-Ray Diffraction	22
3.6	Schematic diagram of X-ray diffractometer	22
3.7	XRD pattern for crystalline sample	23
3.8	XRD pattern for amorphous sample	23
3.9	Energy level diagram showing states involved in Raman spectroscopy	24
3.10	Experimental setup of NOST: HEDA-URSM4/5/7 Raman spectrometer	25
3.11	FTIR instrument SHIMADZU MIRacle 10	26

3.12	**Schematic diagram of SEM**	**27**
3.13	**Experimental setup of SEM**	**28**
3.14	**Experimental setup of HRTEM**	**30**
3.15	**Ray-diagram of double beam spectrophotometer**	**31**
3.16	**JASCO V-670, UV-Vis-NIR spectrophotometer**	**32**
3.17	**Energy level diagram for the electronic transition**	**32**
3.18	**JASCO FP-8200 Spectroflurometer**	**34**
4.1	**DTA curve of the synthesized sample**	**35**
4.2	**Samples after heat treatment**	**36**
4.3	**XRD spectra of synthesized samples**	**37**
4.4	**Raman spectra of synthesized samples**	**38**
4.5	**FTIR spectra of the synthesized samples**	**40**
4.6	**Surface morphology of (A) CTG_0 (B) CTG_4 (C) EDS (D) and elemental mapping (E)CTG_0 particle size and (F) CTG_4 particle size**	**44**
4.7	**(a)HRTEM image of CTG_4 (b) Quantum dot size (c) d-spacing (d) SAED pattern for CTG_4**	**45**
4.8	**UV-Vis spectra of prepared samples**	**46**
4.9	**Tauc's plot of prepared samples**	**47**
4.10	**PL spectra of prepared samples & CIE plot**	**48**
5.1	**UV-Vis absorption spectra of IC dye degradation with CTG_4 using Glass (solid photocatalyst) & glass powder (powder sample)**	**51**

5.2	**Relative concentration of IC dye with irradiation time**	**52**
5.3	**Plot of ln(C_0/C) against irradiation time**	**53**
5.4	**reusability of glass powder (powder sample)&glass sample (solid sample)**	**54**
5.5	**Mechanism of degradation of IC dye using prepared sample**	**57**

LIST OF TABLES

TABLE NO.	PARTICULARS	PAGE NO.
3.1	List of chemicals used	17
4.1	Heat treatment of synthesized samples	36
4.2	FTIR peak shifting with explanation	41
4.3	Energy band gap for prepared samples	47
4.4	Coordinates of CIE plot for all samples.	49
5.1	Determined degradation efficiency and reaction rate of all photocatalysts	53

INDEX

SR. NO.	PARTICULARS	PAGE NO.
	CHAPTER 1 INTRODUCTION	
1.1	Wastewater Pollution	1
1.2	Dyes	2
1.3	Photocatalysis	3
1.4	Why Photocatalysis	3
1.5	Semiconductors in Photocatalysis	4
1.6	Mechanism of Photocatalysis	4
1.7	Quantum Dots	6
1.8	Why Glass	9
1.9	Glass	9
	CHAPTER 2 LITERATURE REVIEW AND METHODOLOGY	
2.1	Literature Review	13
2.2	Objective	15
2.3	Methodology	15

CHAPTER 3

SYNTHESIS OF MATERIAL AND CHARACTERIZATION TECHNIQUES

3.1	Preparation of $CuO-TiO_2$ QDs containing Borosilicate Glass System		17
3.2	Characterization Techniques	DTA study	19
		X-Ray Diffraction Spectroscopy	21
		Raman Spectroscopy	24
		Fourier Transform Infrared Spectroscopy	26
		Scanning electron microscopy	27
		Energy-dispersive X-ray spectroscopy (EDS or EDX)	28
		HRTEM analysis	29
		UV-Vis spectroscopy	30
		Photoluminescence Spectroscopy	32
CHAPTER 4 RESULTS AND DISCUSSION			
4.1	DTA Study		35
4.2	Growth of quantum dots by heat treatment		36
4.3	XRD Analysis		37
4.4	Raman Analysis		37
4.5	Fourier transform infrared Spectroscopy		39
4.6	SEM & EDS Analysis		41
4.7	HRTEM Analysis		44
4.8	UV-Vis Analysis		45

4.9	**Photoluminescence Study**	**48**
CHAPTER 5 PHOTOCATALYTIC ACTIVITY		
5.1	**Experiment**	**50**
5.2	**Result**	**50**
5.3	**Reusability**	**53**
5.4	**Mechanism**	**54**
CHAPTER 6 CONCLUSION AND FUTURE SCOPE		
6.1	**Conclusion**	**58**
6.2	**Future Scope**	**58**
References		

CHAPTER 1

INTRODUCTION

1.1 Wastewater Pollution

Water is one of the most vital resources on Earth, yet its contamination has reached alarming levels due to industrialization, urbanization, and inadequate wastewater management practices. Around 80% of wastewater globally is discharged untreated into natural water bodies, severely compromising freshwater availability [1]. This issue is exacerbated by the rapid depletion of clean water sources, with the United Nations projecting that nearly 5 billion people could face water scarcity by 2050 [1]. Untreated wastewater introduces a mixture of pollutants, including organic compounds, heavy metals, and persistent chemicals, into aquatic ecosystems, posing serious risks to human health and biodiversity. Among these pollutants, synthetic dyes represent a significant environmental challenge [1][2].

Dyes, widely used in industries such as textiles, leather, paper, and food, contribute substantially to water pollution. The textile industry alone is responsible for generating over 700,000 tons of dyes annually, with approximately 10-15% of these dyes discharged into water systems [3]. These dyes contain aromatic molecular structures that are resistant to degradation by natural processes such as photolysis and biodegradation, making them persistent and hazardous [4,5]. Even at low concentrations, dyes reduce water quality by blocking sunlight, which disrupts photosynthesis in aquatic plants and organisms [1][2]. Additionally, they elevate biological oxygen demand (BOD) and chemical oxygen demand (COD), creating oxygen-deprived environments in water bodies [2]. This phenomenon significantly impacts aquatic ecosystems and the organisms dependent on them.

Furthermore, many synthetic dyes are carcinogenic, mutagenic, and bioaccumulative. Azo dyes, for instance, dominate the market yet are particularly harmful due to the release of aromatic amines during degradation processes [2]. Industries that use these dyes release effluents containing harmful substances directly into rivers, lakes, and groundwaters, exacerbating the global water crisis. Managing such pollutants demands innovative

solutions, not only to mitigate their environmental impact but also to align with sustainable development goals for future generations [2,5].

1.2 Dyes

Dyes are coloured organic compounds widely utilized in industries such as textiles, leather, paper, pharmaceuticals, and food processing. Their ability to impart aesthetic and functional qualities stems from their chromophoric groups and stable aromatic structures. These properties make dyes vital in industrial applications, but also render them resilient pollutants in wastewater systems, contributing to environmental degradation [6,7].

1.2.1 Classification of Dyes

Dyes are broadly categorized based on their origin, chemical composition, and application:

1) **Natural Dyes**: Derived from organic sources such as turmeric and indigo. While eco-friendly, their limited chemical stability restricts widespread industrial usage [7].
2) **Synthetic Dyes**: These dyes dominate industrial applications due to their durability and adaptability. Subcategories include:
    - ❖ **Acid Dyes**: Commonly used for silk and wool applications.
    - ❖ **Basic Dyes**: Utilized in the textile, leather, and paper industries.
    - ❖ **Reactive Dyes**: Known for strong covalent bonding with fibres, providing colourfastness.
    - ❖ **Azo Dyes**: Representing a significant portion of global dye production, these are versatile but environmentally persistent.
    - ❖ **Vat Dyes**: Ideal for cotton dyeing due to their solubility.

Of specific concern are **organic dyes**, these are part of the synthetic dye category. These dyes are characterized by aromatic hydrocarbon structures, including benzene, toluene, and anthracene. They resist conventional wastewater treatment due to their complex aromatic rings, making them stable against photodegradation, oxidation, and microbial decomposition.

1.2.2 Methods for Dye Removal

The challenge of removing dyes from wastewater has led to the development of various methods, broadly categorized into physical, chemical, and biological processes.

1. **Physical Methods**: Techniques like adsorption using activated carbon and membrane filtration are widely used. These methods are effective at extracting dyes from water, but often lead to secondary pollution in the form of concentrated waste [6,8].
2. **Chemical Methods**: Processes such as oxidation (e.g., Fenton reactions) and coagulation/flocculation break down or aggregate dye molecules. However, these approaches can produce toxic byproducts and require significant energy or chemical inputs [4].
3. **Biological Methods**: Microbial or enzymatic treatment uses microorganisms or enzymes to degrade dyes. These methods are environmentally friendly, but slow and often limited by the structure of complex dyes like azo compounds [1,5].

1.3 Photocatalysis

Among the available techniques, photocatalysis stands out due to its ability to achieve complete dye degradation efficiently and sustainably. **It** has emerged as a highly effective, sustainable, and innovative approach. This technique utilizes light energy—typically UV or visible light—to activate semiconductor catalysts, such as titanium dioxide (TiO_2), zinc oxide (ZnO), and advanced materials like quantum dots, for the complete mineralization of dyes into harmless products such as CO_2 and water [8,9].

1.4 Why Photocatalysis?

- **Complete Degradation**: Unlike physical methods, photocatalysis breaks down dye molecules entirely, eliminating risks of secondary pollution [8].
- **Eco-Friendliness**: The process harnesses light energy, including sunlight, reducing reliance on chemicals and energy-intensive processes [9].
- **Efficiency with Organic Dyes**: Photocatalysts can effectively degrade even persistent organic dyes, overcoming the limitations of chemical and biological methods [1,2].

- **Reusable Catalysts**: Advanced materials like TiO_2 and ZnO composites are stable and reusable, making the method cost-effective [11].

This thesis focuses on enhancing the efficiency of photocatalysis by integrating semiconductor quantum dot composites with metals, offering a scalable and innovative solution to combat dye pollution.

1.5 Semiconductors in Photocatalysis

Semiconductors play a pivotal role in photocatalysis, a process that mimics aspects of photosynthesis by utilizing light energy to drive chemical reactions. These materials, such as titanium dioxide (TiO_2), zinc oxide (ZnO), and cadmium sulfide (CdS), are characterized by their unique electronic structures, which include a filled valence band and an empty conduction band separated by a bandgap. When exposed to light with energy equal to or greater than this bandgap, semiconductors absorb photons, generating electron-hole pairs that initiate redox reactions. Key points include:

- **Light Absorption**: Semiconductors absorb photons, exciting electrons from the valence band to the conduction band.
- **Charge Separation**: The generated electron-hole pairs are spatially separated to prevent recombination.
- **Catalytic Activity**: These charge carriers interact with adsorbed molecules, facilitating oxidation and reduction reactions.

1.6 Mechanism of Photocatalysis

Electronic energy levels are continuous in metals. Their valence and conduction bands overlap. A void, however, extends from the molecule orbital with highest energy occupied by the electrons, referred as the HOMO, to the lowest unoccupied molecular orbital, known as the LUMO, in semiconductors [10]. Consequently, the energy band—a space between the valence and conduction bands—exists. An excited electron from the valence band moves to the conduction band and leaves a hole in the valence band when this semiconductor is exposed to radiation with energy greater than or equal to E_g.

Assume that this semiconductor absorbs photons with energy equal to hv when exposed to radiation. An electron from the valence band will be stimulated to the conduction band after creating a hole in the valence band if this energy is the same as or exceeding than the band gap energy.

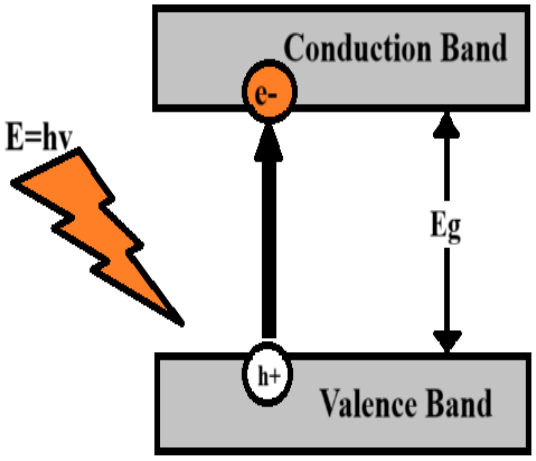

Fig 1.1 Electron-Hole production

For TiO_2, when irradiated by photons, the reaction can be written as:

$$h\upsilon + TiO_2 \longrightarrow e_{CB}^{-} + h_{VB}^{+}$$

The primary mechanism of the photocatalysis process is the above-shown chemical reaction. Normally, the hole facilitates the oxidation of water, producing hydroxyl radicals, which start a sequential reaction that oxidizes organic contaminants. An electron acceptor will receive the electron. An electron interacts with oxygen to produce a superoxide ion or lowers the metal ion to its most reduced oxidation state, which is then deposited on the catalyst's surface.

$$H_2O + h\upsilon^{+} \longrightarrow H^{+} + {}^{\cdot}OH$$

$$O_2 + e_{CB}^{-} \longrightarrow O_2^{-}$$

$$H_2O + O_2^{-} \longrightarrow {}^{\cdot}OOH + OH^{-}$$

$$H^{+} + {}^{\cdot}OOH \longrightarrow OH^{-} + {}^{\cdot}OH$$

$$H_{VB}^{+} + OH^{-} \longrightarrow {}^{\cdot}OH$$

$${}^{\cdot}OH + Pollutant \longrightarrow CO_2 + H_2O$$

The hydroxyl radical (•OH) actively attacks pollutants. The complete chemical processes are illustrated in the figure.

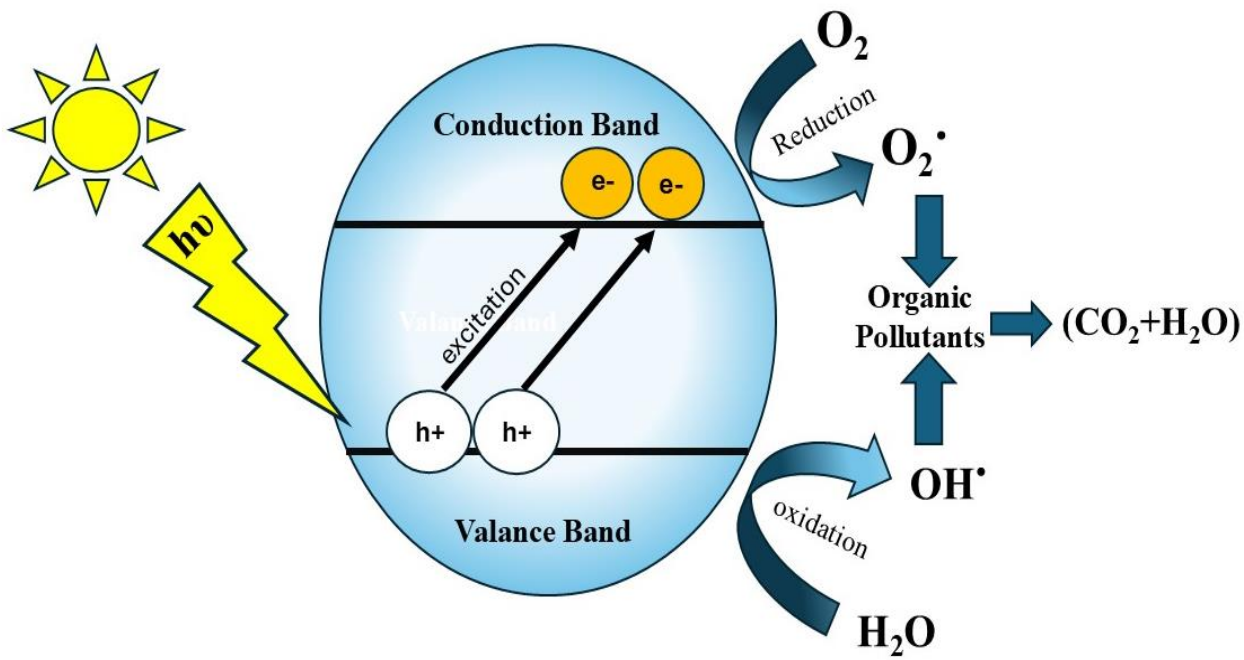

Fig. 1.2 Mechanism of photocatalyst

1.7 Quantum Dots

Quantum dots (QDs) are nanoscale semiconductor particles, typically ranging from 2 to 10 nanometres in size. These particles exhibit unique optical and electronic properties due to quantum confinement effects, which occur when the particle size becomes comparable to the de Broglie wavelength of electrons. This confinement leads to discrete energy levels, similar to those in atoms, earning quantum dots the nickname "artificial atoms." Their optical properties, such as light absorption and emission, are size-dependent, allowing them to emit specific wavelengths of light when excited. For instance, smaller quantum dots emit shorter wavelengths (blue light), while larger ones emit longer wavelengths (red light).

Quantum dots were first discovered in the late 1970s by Alexei Ekimov, who observed quantum size effects in nanocrystals. This was followed by Louis Brus synthesizing colloidal quantum dots in the early 1980s, and Alexander Efros providing theoretical explanations, laying the foundation for their unique optical and electronic properties. Over

time, advancements in synthesis techniques have expanded their applications across fields like optoelectronics and environmental science

Quantum dots are widely used in applications like display technologies (e.g., QLED TVs), solar cells, biological imaging, and photocatalysis due to their tunable properties and high efficiency in light absorption and emission.

1.7.1 Classification of Quantum Dots

- **Core Quantum Dots**: These are single-component quantum dots that rely on size-dependent quantum confinement effects for their properties.
- **Core-Shell Quantum Dots**: Have a core material (e.g., CdSe) surrounded by a shell (e.g., ZnS) to enhance photoluminescence and protect against degradation.
- **Alloyed Quantum Dots**: Composed of a mixture of semiconductor materials, offering intermediate bandgaps and improved tunability of optical properties.
- **Doped Quantum Dots**: Incorporate specific ions (e.g., transition or rare-earth ions) into the quantum dot lattice to introduce new electronic or magnetic properties.

1.7.2 Properties of Quantum Dots

1) **Size-Dependent Optical Properties**: The emission wavelength of quantum dots depends on their size. Smaller dots emit shorter wavelengths (blue light), while larger dots emit longer wavelengths (red light).
2) **High Photoluminescence**: Quantum dots have a high quantum yield, meaning they efficiently convert absorbed light into emitted light.
3) **Tunable Bandgap**: Their bandgap can be adjusted by changing their size, enabling precise control over their electronic and optical behaviour.
4) **Stability**: Quantum dots are resistant to photobleaching, making them ideal for long-term applications like imaging.
5) **Versatility**: They can be engineered for specific applications by altering their composition, surface ligands, or doping with other materials.

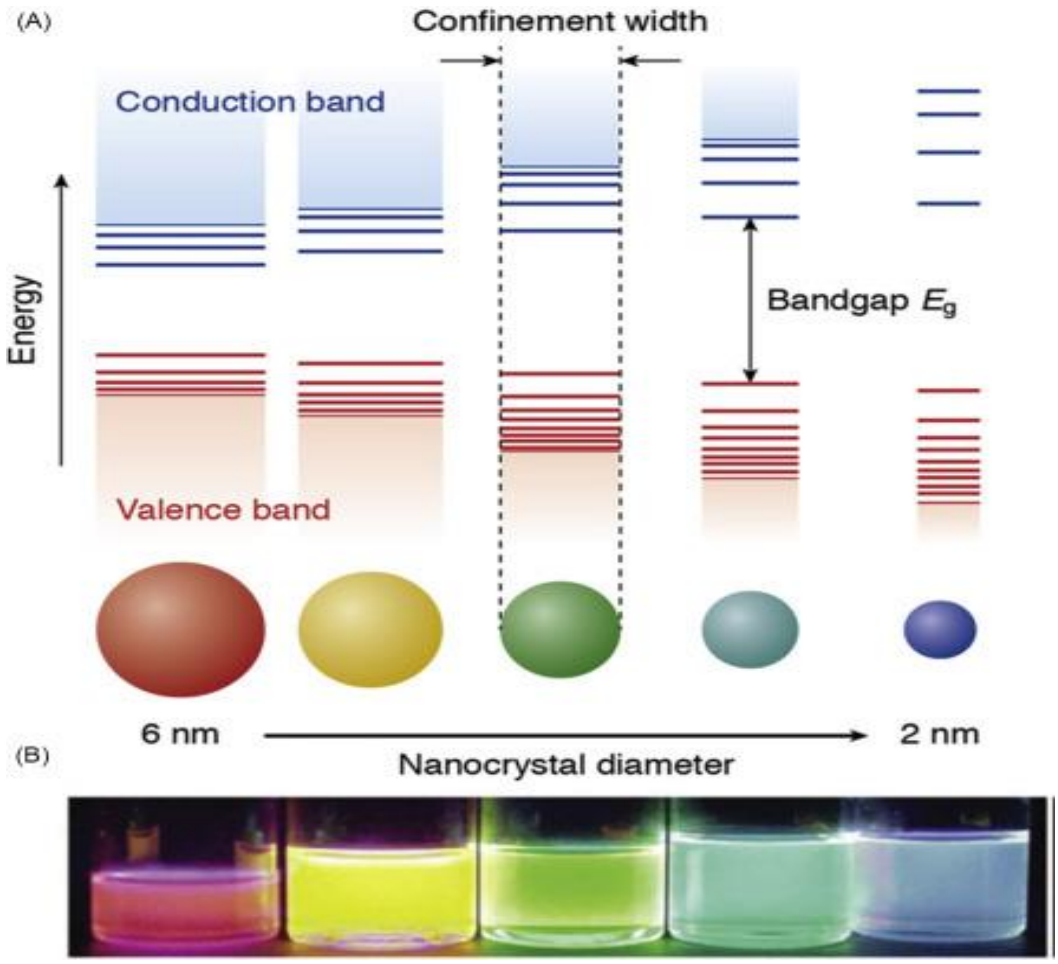

Fig 1.3-Dimensional dependence of quantum energy levels

1.7.3 Applications of quantum dots

Quantum dots, owing to their exceptional properties, have been applied across a wide range of fields, including the conversion of carbon dioxide into hydrocarbons. Researchers at Rice University have demonstrated that nitrogen-doped quantum dots can function effectively as catalysts. Meanwhile, scientists at Los Alamos National Laboratory have utilized cadmium-indium selenide sulfide quantum dots to develop cost-effective solar cells. Magnetic quantum dots have been engineered for use in memory storage and spintronic devices. Various companies have incorporated quantum dots into the production of television and computer displays, achieving enhanced color efficiency. Additional applications extend to quantum light-emitting diodes (QLEDs), solid-state lighting, photovoltaic systems, and quantum computing, where they contribute to the development of qubits.

1.7.4 Limitations of quantum dots

Quantum dots face challenges, including agglomeration, where particles cluster together, compromising their properties and functionality. Achieving homogeneity during synthesis is crucial, as variations in size, shape, or composition can disrupt their predictable performance. Impurities introduced during synthesis can reduce quantum yield and introduce unwanted effects, such as non-radiative recombination. Moreover, instability due to external factors like light, temperature, and moisture leads to photoluminescence loss and blinking phenomena, limiting their long-term use. To overcome these limitations, QDs should be embedded in a solid matrix. QDs embedded in glass show better results [11].

1.8 Why glass

Embedding quantum dots in glass enhances their stability by shielding them from environmental factors like moisture and temperature, preventing agglomeration and ensuring uniform dispersion. The glass matrix minimizes impurities, preserves optical properties, and enables tunable emission for advanced applications. Since glass is a transparent and chemically inert solid matrix and thermally stable, it can be used to incorporate quantum dots.

1.9 Glass

As we are incorporating QDs in glass, we should know what glass is. Glass is a supercooled liquid. It is classified as an amorphous solid, meaning it lacks a long-range ordered crystalline structure. This unique property distinguishes glass from other solid materials and contributes to its remarkable characteristics, such as transparency, brittleness, and versatility. Glass exhibits time-dependent glass transformation behaviour. Glass is usually an inert material and is resistant to chemical attacks [12].

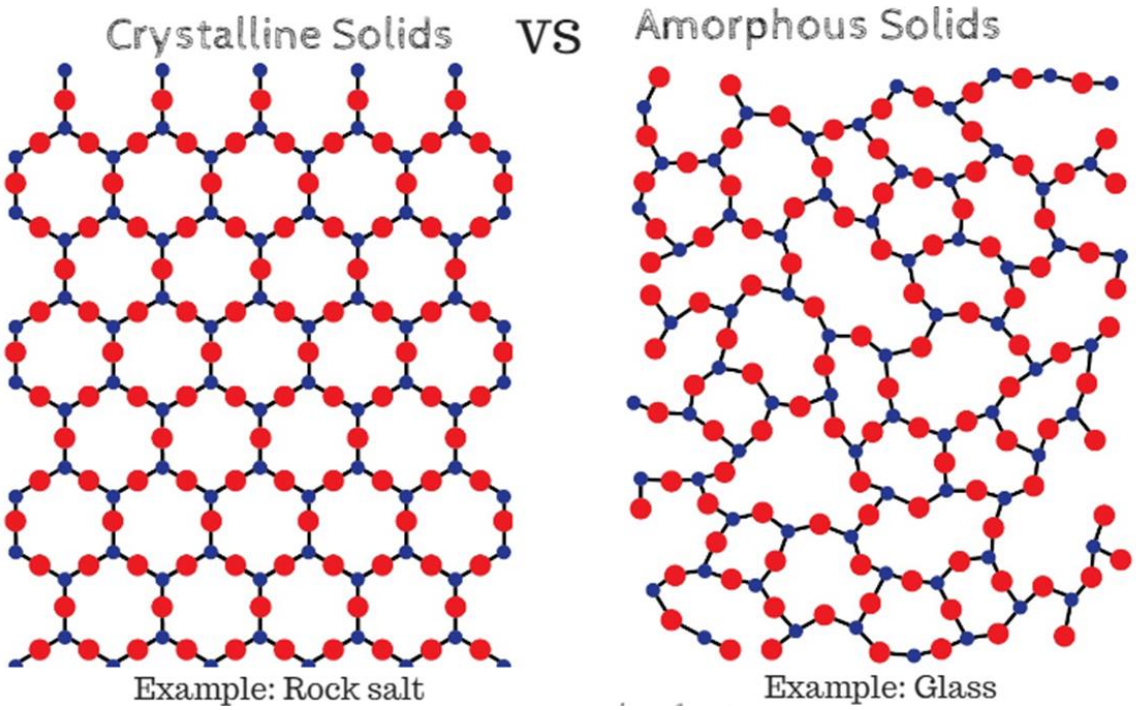

Fig. 1.4 crystalline and amorphous structures

1.9.1 Glass structure

(1). Formers

Formers are the primary components that constitute the glass network. These materials form the backbone of the glass structure by creating a continuous, rigid network through covalent bonding. examples include boron oxide (B_2O_3) and phosphorus pentoxide (P_2O_5).

(2). Modifiers

Modifiers are added to disrupt the glass network, making it more workable and altering its properties. They do not form part of the primary glass network but instead occupy the interstitial spaces, weakening the network structure. Examples include sodium oxide (Na_2O) and potassium oxide (K_2O)

(3). Intermediates

Intermediates can function as both formers and modifiers, depending on the conditions of the glass formation. These components improve the chemical durability, mechanical strength, and optical properties of the glass. Examples include alumina (Al_2O_3) and titanium dioxide (TiO_2).

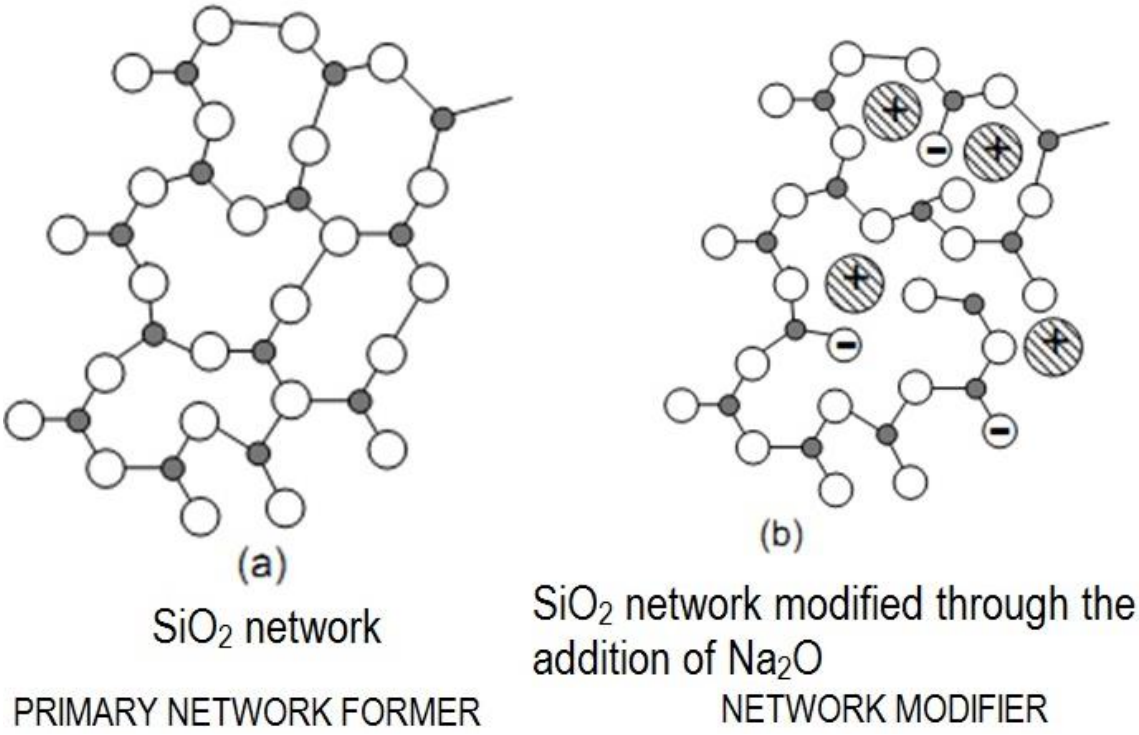

Fig. 1.5 Components of glass

1.9.2 Glass formation

The process of glass formation can be illustrated using a graph of volume or enthalpy versus temperature. When a liquid is cooled below its melting point, a new phase begins to form. The characteristics of this phase are influenced by the rate of cooling. Under slow cooling conditions, atoms have sufficient time to periodically rearrange themselves, leading to the crystallization of the liquid into an ordered solid structure. The temperature at which this transition occurs is known as the crystallization temperature (Tc), with quartz serving as a common example of such a process.

In contrast, when the cooling is rapid—often referred to as quenching—the atoms lack the mobility to organize into a crystalline structure. This results in the formation of a rigid, amorphous solid known as glass. The point at which a supercooled liquid shifts from a rubbery or viscous state to a hard, amorphous solid is called the glass transition temperature (Tg). This temperature is a key characteristic of ceramic materials. Understanding both the glass transition temperature and the crystallization temperature is essential when working with glassy systems.

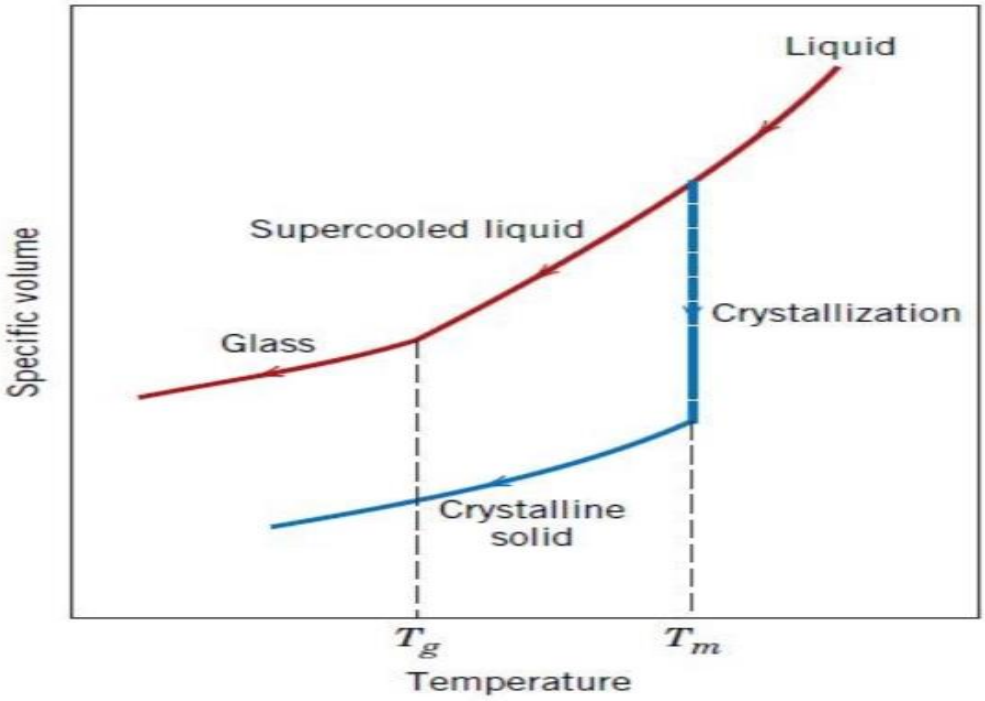

Fig. 1.6 Volume vs Temperature graph of glass formation

CHAPTER - 2

LITERATURE REVIEW and OBJECTIVE

2.1 Literature Review

This project aims to degrade organic dyes that contaminate water. Therefore, several studies have been reviewed to determine the appropriate synthesis technique for sample preparation and application for photocatalysis. This chapter summarizes the relevant literature that forms the foundation for this research work.

- **S.Y. Janbandhu et al**. [11]- A glass system containing CdS and ZnS prepared using the melt quench method. Glasses were heat-treated to grow CdS/ZnS QDs. The variation of the energy band gap with respect to quantum dot size was investigated and characterized through optical techniques. Prepared samples were tested as a photocatalysts under sunlight for the degradation of indigo carmine (IC) dye, and photodegradation efficiency was found to be 73.6 % and 87.2 % for samples CZ1 and CZ4, respectively. No significant change is observed in degradation efficiency even for 4 cycles, confirming the prepared glasses' stability for dye degradation.
- **Ayesha Sabir et al.** [13]- Ag-doped TiO_2 nanoparticles embedded in a porous polymer (PPTS) were prepared using an in-situ solvothermal process. The degradation ability of PPTS under xenon light as well as natural sunlight is analysed and compared with bare TiO_2 and Ag-TiO_2 for the degradation of methyl orange. The photocatalytic activity of the prepared sample for methyl orange dye was improved under visible light irradiation. The developed photocatalyst (PPTS) system can easily be recovered, and its photocatalytic efficiency is retained at almost 97% up to 10 cycles, which makes the developed system a potential and sustainable solution for pollution abatement.
- **Osman Örneka et al.** [14] - Europium-doped titanium dioxide thin film, fabricated via the sol-gel method, was used as electron transport layers in inverted organic solar cells. Eu: TiO_2 thin films were fabricated with different Eu concentrations as 0, 1, 5, 7, and 10% (w/w). The effect of Eu doping concentration on the photovoltaic performance of the inverted-type solar cells was studied. The power conversion efficiency of the fabricated solar cells increased from 1.16% to 2.47%

at 5% Eu doping concentration. The electron transport and hole-blocking properties of the TiO_2 interlayer were improved by Eu doping.

- **Yuxiang Zhu et al.** [15]- CdS quantum dots (QDs) were deposited on TiO2 nanotube arrays (TNTAs) using the successive ionic layer adsorption and reaction (SILAR) method for visible-light-driven hydrogen production and organic compound degradation. The loading amount of CdS was adjusted by controlling the deposition cycles, which demonstrated optical behaviours. CdS-TNTAs sample prepared by SILAR deposition with 15 cycles gives the highest hydrogen production rate of 1.89 mol h−1 cm−2 for 15 mL solutions and the highest degrading rate. The prepared sample had good stability and could be more easily reused than the powder catalyst
- **P.P. Pawar et al.** [16]- Eu_2O_3doped Li_2O–Ag_2O_3–B_2O_3 glasses (LABE) were synthesized by the melt quenching technique for solid-state lighting applications. The glasses were synthesized with chemical composition $30Li_2O{\cdot}10Si_2O{\cdot}(60 - x)$ $B_2O_3{\cdot}xEu_2O_3$ where x = 0.0, 0.2, 0.4, 0.6, 0.8 mol %. The CIE chromaticity diagram showed that glass LABE-4 (0.8 mol% Eu) shows the highest emission intensity among all glass samples.
- **S.R. Munishwar et al.** [17] have studied the synthesis of CdS quantum dots (QDs) embedded in a boro-silicate glass matrix (SiO_2-B_2O_3-ZnO-Na_2O-K_2O) through a controlled heat treatment process to analyze the influence of electron-hole recombination on the optical properties of the quantum dots. The experiment shows that the CdS QD size is very well controlled by single-stage heat treatment. Size-dependent blue shift in the optical energy band gap was observed. Therefore, these glasses can be used as an optical filter in devices
- **Ashwini S. Gadge et al.** [18] - Cerium-doped TiO_2 nanoparticles via a sol-gel method were synthesized using titanium tetraisopropoxide as the precursor material to improve environmental applications such as water purification, self-cleaning surfaces, and antibacterial activity. The synthesis material was verified through characterization techniques like XRD, Raman, HR-TEM, and XPS. Results revealed high photocatalytic efficiency (97.08% for methylene blue dye degradation), superhydrophilic self-cleaning surfaces, and significant antibacterial properties, demonstrating the material's effectiveness in sustainable environmental solutions.

- **Chun-ying Huang et al.** [19]- Eu-doped TiO_2 nanoparticles via the sol-gel method to enhance the photocatalytic reduction of CO_2 into CH_4 and CO under visible light, addressing environmental concerns like CO_2 emissions and energy sustainability. The synthesis was confirmed using techniques such as XRD, SEM, TEM, EDS, UV-Vis spectroscopy, and photoluminescence. The results showed that the 0.25% Eu-TiO_2 catalyst achieved significantly improved yields of CH_4 and CO (65.53 and 42.91 μmol/g.cat, respectively), highlighting its superior photocatalytic efficiency due to better visible light absorption and electron-hole separation.

2.2 Objective

From the literature it is reviewed that many methods are available for waste-water treatment, but none have 100% efficiency therefore very economical and efficient method of photocatalysis using semiconductor quantum dots has been chosen for water treatment.

Some widely used semiconductor photocatalysts include TiO_2, ZnSe, CdS, and ZnS. These materials possess wide band gaps, meaning they require high-energy input to generate electron-hole pairs. As a result, they can only be activated by ultraviolet (UV) light, which is less energy-efficient and more expensive compared to visible light.

To use TiO_2 in visible light, it is essential to reduce or modify the bandgap, and this can be possible by doping. In the present work attempt is to make TiO_2 as a catalyst in the glass system by co-doping with CuO. Numerous studies have been conducted in this area; however, research focus on CuO/TiO_2 heterojunction embedded in glass for photocatalytic applications remains limited. Therefore, the objective of this project is to develop CuO/TiO_2 heterojunction quantum dots in glass matrix for water treatment. Accordingly, the proposed title is "A facile synthesis of binary CuO/TiO_2 heterojunction in glass matrix as photocatalyst for dye degradation."

2.3 Methodology

Project work is carried out using the following methodology: -

- Synthesis of glass with CuO/TiO_2 heterojunction by the melt and quench method.

- To determine glass transition temperature using DTA.
- XRD of these glasses to confirm the amorphous nature.
- Heat Treatment of glasses for the growth of quantum dots.
- FTIR of glasses..
- RAMAN analysis.
- SEM and EDS analysis
- HRTEM before and after heat treatment.
- UV-Visible Absorption measurement before and after heat treatment.
- PL measurement before and after heat treatment.
- CIE analysis.
- Photocatalysis study.

Chapter 3

Synthesis of Material and Characterization Technique

This section details the materials, procedures, and equipment used for the synthesis and characterization of CuO/TiO_2 quantum dots embedded in glass matrix, along with the various stages involved in the experimental process.

3.1 Preparation of CuO-TiO_2 QDs containing Borosilicate Glass System

To prepare the borosilicate glass system, high-purity chemical precursors were used. Silicon dioxide (SiO_2) and boron oxide (B_2O_3) acted as the primary glass formers, while sodium oxide (Na_2O) and potassium oxide (K_2O) were incorporated as network modifiers. Aluminum oxide (Al_2O_3) served as an intermediate to enhance the chemical durability and structural stability of the glass network. These components were accurately weighed and mixed to form a total batch of 10 grams.

To introduce semiconducting properties for quantum dot formation, 2 weight percent (wt%) of copper(II) oxide (CuO) and 1 wt% of titanium dioxide (TiO_2) were added to the base glass composition. The precise quantities of each raw material used in the formulation are provided in Table 3.1.

Table 3.1 List of chemicals used.

Sr. no	Chemical	Make	Purity	Molar mass (g/mol)	Mol%/wt%
1.	SiO_2	Sigma-Aldrich	≥99%	60.08	47 Mol%
2.	B_2O_3	Merck	≥99.7%	69.61	25 Mol%
3.	Na_2O	Merck	≥99.9%	105.99	15 Mol%
4.	K_2O	Merck	≥99.5%	138.21	10 Mol%
5.	Al_2O_3	Sigma-Aldrich	≥98%	101.96	3 Mol%

6.	CuO	Sigma-Aldrich	99.0%	79.55	2 Wt%
7.	TiO_2	Sigma-Aldrich	99.99%	79.86	1 Wt%

The chemical precursors were precisely weighed using a high-accuracy and highly sensitive analytical balance (SHIMADZU AUW220D). The measured chemicals were then transferred to a thoroughly cleaned agate mortar with the help of butter paper, which had been pre-washed using acetone to eliminate any contaminants. Using a pestle, the materials were ground and mixed thoroughly to ensure a homogeneous blend. The resulting mixture was carefully placed into a platinum crucible and introduced into a high-temperature electric furnace. The batch was melted at 1200 °C for a duration of three hours to achieve complete fusion and refinement of the glass-forming materials. Following melting, the molten glass was quickly air-quenched by pouring it onto an aluminum mould at room temperature. This rapid cooling was immediately followed by an annealing process at 330 °C for 2-2.5 hr to relieve the internal thermal stresses developed during quenching. The glass was then allowed to cool gradually to room temperature inside the annealing furnace to complete the synthesis process. A schematic representation of the entire synthesis procedure is provided in Figure 3.1.

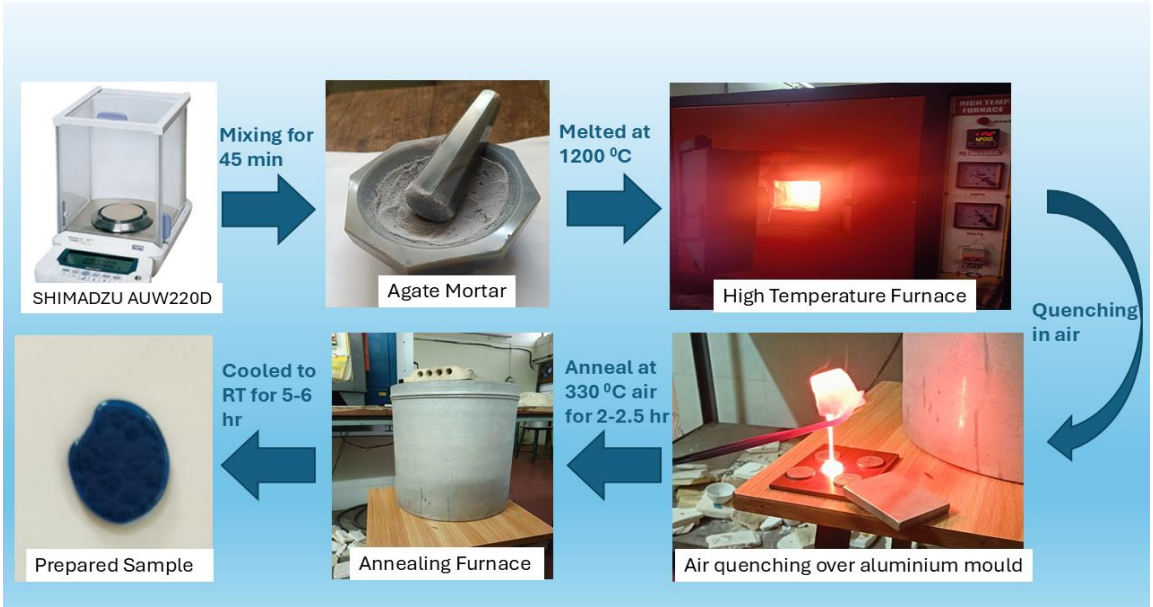

Fig 3.1. Schematic representation of the synthesis of glass by the Melt Quench Method.

3.2 Characterization Techniques

After the synthesis of the materials, the various properties of materials, like physical, chemical, and optical, are very important to be studied. There are various characterization techniques to know the different properties of the materials. In the present work, QDs embedded in glasses are characterized, and some techniques were used to analyze thermal properties, crystallinity, surface morphology, optical properties, etc.

The techniques are:-

1. DTA study
2. X-Ray diffraction spectroscopy
3. Raman spectroscopy
4. FTIR spectroscopy
5. SEM and EDS analysis
6. HRTEM analysis
7. UV-Vis spectroscopy
8. Photoluminescence analysis

Information related to these techniques is given below.

3.2.1. DTA (Differential Thermal Analysis)

Differential thermal analysis is very important and a primary characterization in the whole characterization. This technique is utilized to determine the glass transition temperature (T_g) and crystallisation temperature (T_c) of the glass. A schematic of DTA is shown in Figure 3.2. In this technique, the sample and the reference are heated and cooled identically, and the temperature difference is recorded. The temperature difference is called differential temperature. This temperature difference is plotted against temperature or time. [20]. The peak on this graph will give the value of T_g and T_c. DTA is also used for the study of phase transitions and thermal analysis of the material.

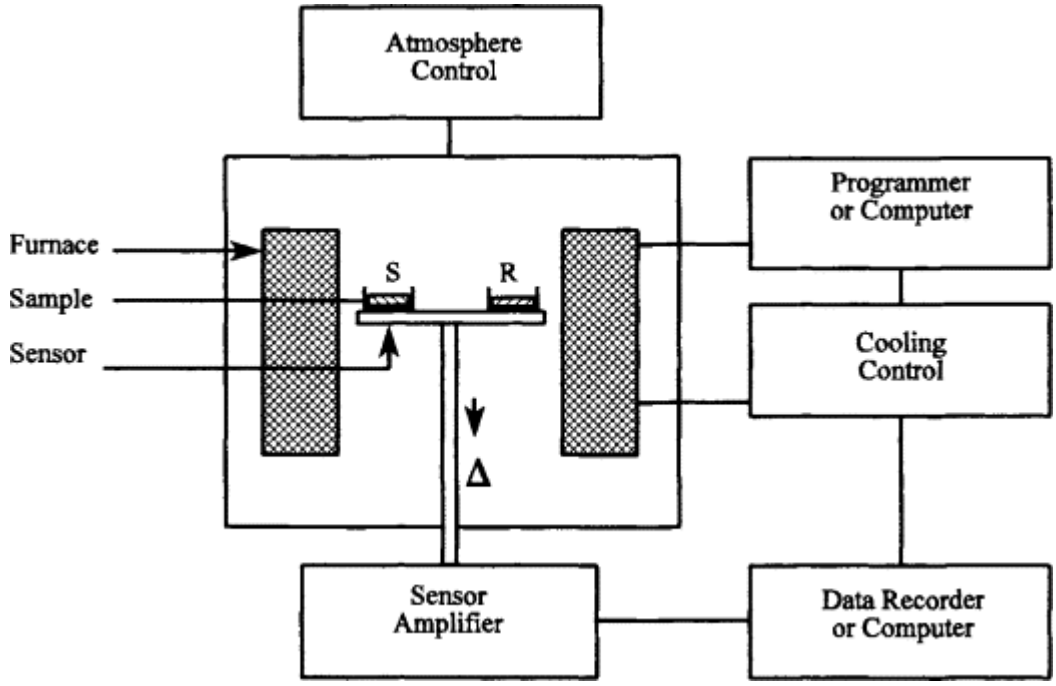

Fig. 3.2 Schematic diagram of differential thermal analysis

It consists of a sample holder and a reference. The thermocouple is attached separately to both the sample and reference for the indication of temperature. The temperature difference is measured, and finally plot is made between the temperature difference and temperature. A plot for DTA measurement is shown in Fig. 3.3

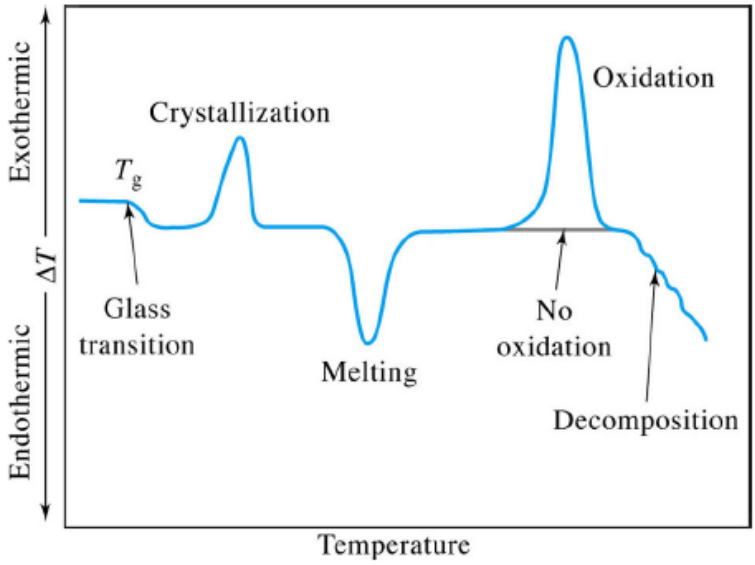

Fig. 3.3 DTA curve

The differential thermal analysis DTA measurement of the prepared sample was done using STAT7200 HITACHI, JAPAN(Fig. 3.4)

Fig 3.4 STAT7200 HITACHI, JAPAN

3.2.2 X-ray diffraction

X-ray diffraction, often referred to as X-ray crystallography, is a widely used technique for investigating the atomic and crystal structure of materials. In this method, a focused beam of X-rays is directed onto a sample, leading to the generation of diffraction patterns. By analyzing the angles and intensities of the diffracted beams, a three-dimensional map of electron density within the material can be constructed. This electron density distribution provides valuable insights into atomic positions, bonding structures, and the periodic arrangement of atoms within the crystal lattice.

There are two main types of X-ray diffraction methods: single-crystal XRD and powder XRD. The fundamental principle underlying X-ray diffraction is Bragg's Law, which governs the condition for constructive interference: $\mathbf{n\lambda=2d \sin \theta}$, where λ is the wavelength of the incident X-rays, θ is the angle of diffraction, d is the spacing between atomic planes, and n is an integer representing the order of reflection [21,22]. By analyzing the intensities of the scattered X-rays, a detailed diffraction pattern is obtained, which can be interpreted to reveal the material's structural characteristics.

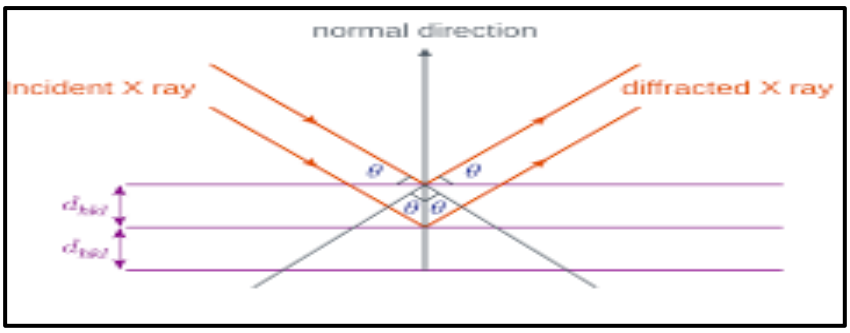

Fig. 3.5 X-Ray Diffraction

The primary instrument used for this analysis is a diffractometer, which consists of an X-ray source (tube) and a detector that moves around the sample in a circular path. A schematic of the diffractometer setup is illustrated in Figure 3.6, while the general working principle is outlined in Figure 3.5

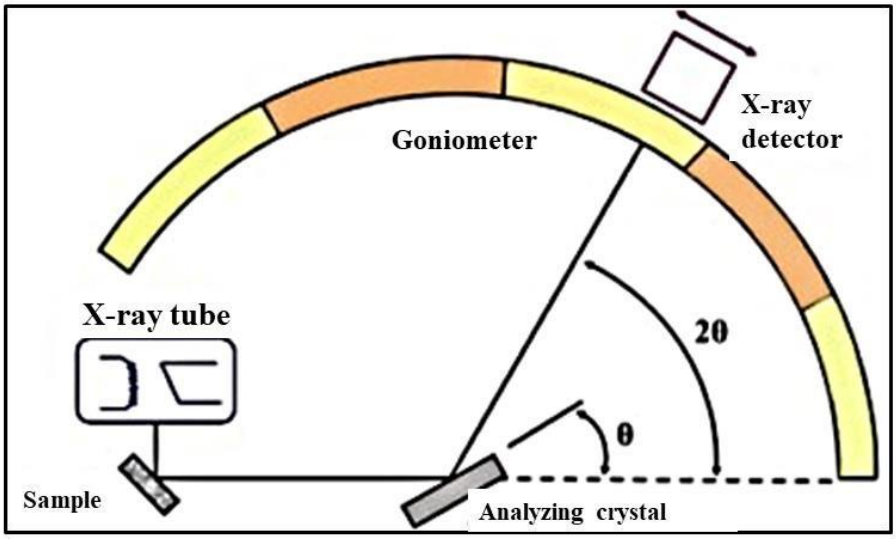

Figure 3.6 Schematic diagram of X-ray Diffractometer

The detector records the intensity of scattered X-rays at varying angles. These measurements are plotted as a graph of intensity versus 2θ, as shown in Figures 3.7 and 3.8

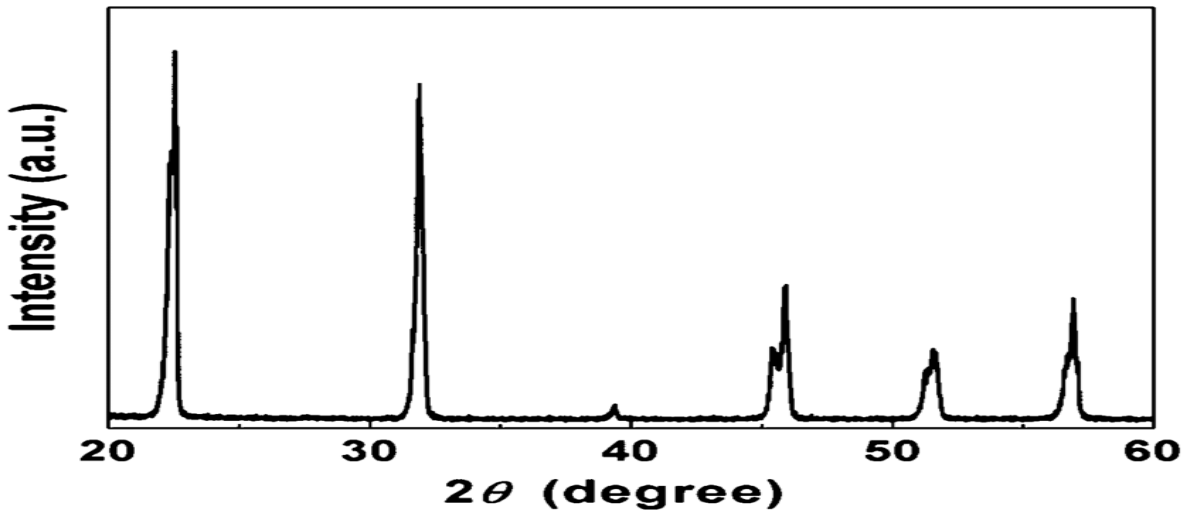

Fig. 3.7 XRD pattern for crystalline sample

In such patterns, the presence of sharp peaks indicates crystalline phases and a periodic atomic arrangement. Conversely, the absence of distinct peaks suggests an amorphous structure, which lacks long-range periodicity. Amorphous materials, such as glasses, typically produce broad, featureless diffraction patterns.

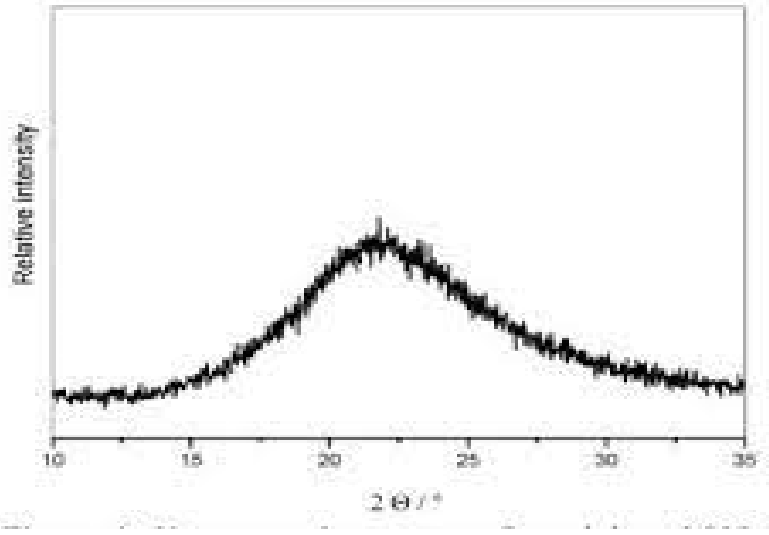

Fig. 3.8 XRD pattern for Amorphous sample

3.2.3 Raman Analysis

Raman Spectroscopy is widely used non-destructive tool for exploring how atoms and molecules behave in solids, liquids and gases. It is helpful in identifying vibrational modes. It is also useful in analysis of phase, and physical interactions like electron-phonon or spin-phonon coupling as well as phase transitions.

This technique works by shining a laser- light of a single wavelength onto a sample. While most of this is reflected unchanged, a tiny portion of it changes in energy after interacting with the sample. This energy shift is known as inelastic scattering, is the core of Raman effect. The change in light frequency gives information about molecules vibrational and rotational characteristics, including low-energy excitations.

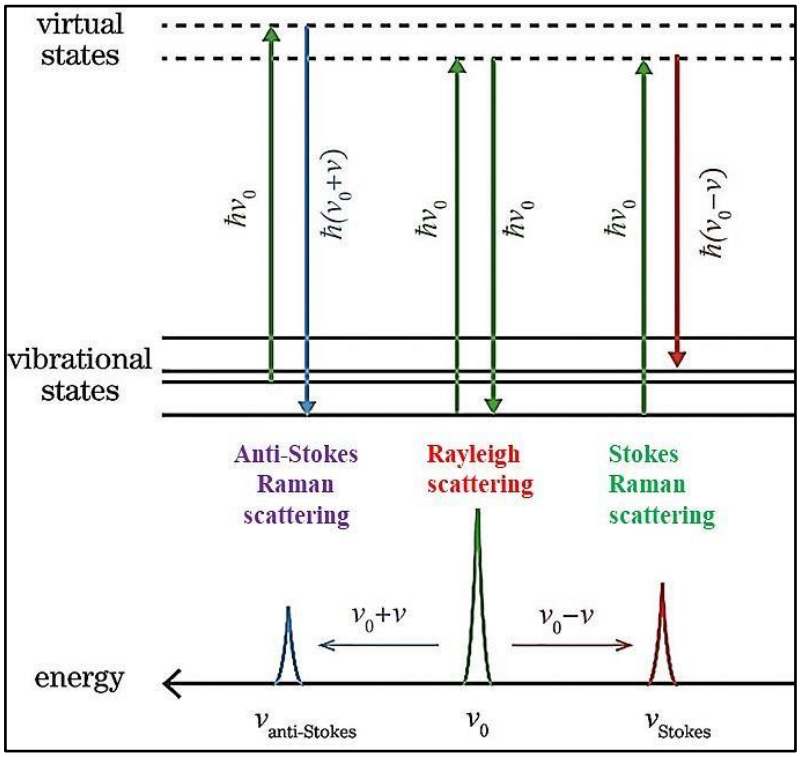

Fig. 3.9 Energy level diagram showing states involved in Raman spectroscopy

This effect is causes temporary distortion of the molecule's electron cloud when it's exposed to the laser's electric field. This distortion depends on how "polarizable" the molecule is i.e. how easily its charge distribution can be shifted. Molecular distortion in the electric field gives molecular polarizability(a), which is the basis of the Raman effect.

Depending on the interaction, three different types of scattered light can be observed:

1. Rayleigh scattering: This is elastic scattering where the molecule stays in its original vibrational state. The energy of the incoming and scattered light remains the same. Materials that don't have Raman-active modes will mostly show this kind of scattering.
2. Stokes Scattering: This occurs when the molecule absorbs some of the laser's energy and gets excited to a higher vibrational level. The scattered light has less energy than the incident light, which makes its frequency lower (vo-vm). This is the most common form of Raman scattering observed.
3. Anti-Stokes scattering: In this case, the molecule is already in an excited state when the laser hits it. It gives up some of that energy to the scattered light, so the outgoing light ends up with more energy than it started with, hence resulting in a higher frequency (Vo + Vm) [23]

Fig. 3.10 Experimental setup of NOST: HEDA-URSM4/5/7 Raman spectrometer

Raman spectroscopy is performed by HEDA-URSM4/5/7 (Fig.(3.10)) at room temperature using an excitation source as LASER of 532 nm wavelength in this project work.

3.2.4. Fourier Transform Infrared Spectroscopy (FTIR)

Fourier Transform Infrared Spectroscopy (FTIR) is a widely used characterisation technique for identifying functional groups and analyzing molecular structures based on vibrational transitions in chemical bonds. It measures the absorption of infrared radiation, producing a spectrum unique to the sample's chemical composition. Each type of bond or functional group in a molecule absorbs infrared light at characteristic frequencies, producing a spectrum that serves as a molecular fingerprint of the material.

FTIR is non-destructive, requires minimal preparation, and is suited for solids, liquids, and thin films. It was used to confirm the presence of specific functional groups and to verify chemical modifications during synthesis. It is specially used for analysing organic compounds, polymers, and composite materials. One of the most common sampling methods used is Attenuated Total Reflectance (ATR), which simplifies analysis by allowing direct contact between the crystal and the sample surface.

In research involving material synthesis or surface modification, FTIR helps track changes in chemical structure by monitoring the appearance, disappearance, or shift of specific absorption bands. Overall, FTIR provides semi-quantitative insights into a material's chemical composition and structural changes [24,25].

Fig. 3.11 FTIR instrument SHIMADZU MIRacle 10.

3.2.4 Scanning Electron Microscopy (SEM)

Scanning Electron Microscopy, or SEM, is a highly effective method used to explore the surface features of various materials at a microscopic level. This uses a a tightly focused beam of electrons that is systematically moved across the sample's surface.

These electrons are generated either by heating a filament or through field emission. Once emitted, electromagnetic lenses are used to accelerate and steer the electron beam so that it hits specific spots on the materials with great precision. As the electrons interact with the atoms on the surface, they generate various signals- mainly secondary electrons, backscattered electrons and characteristics X-rays. These tells us about the surface's, composition, and topography. The secondary electrons, produces highly detailed images that reveal the nanoscale structure of a sample.

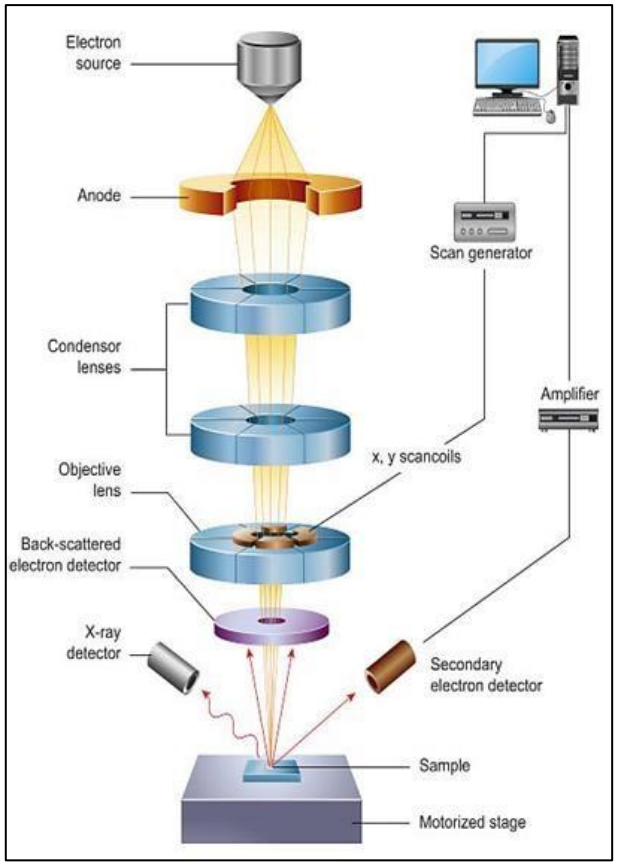

Fig. 3.12 Schematic diagram of SEM

These signals are picked up by sensitive detectors and turned into digital data. Advanced software then processes this data to create a sharp, detailed image. As SEM uses electrons instead of light, it can achieve magnifications much better than a traditional microscope. Its major advantage is that it doesn't damage the sample during imaging [26]. This makes it ideal for analyzing delicate or valuable materials. All the SEM pictures were taken from the ―ZEISS evo SEM18‖ SEM instrument in this project work. A schematic representation of the device and experimental setup is shown in the figure. 3.12.

Fig. 3.13 Schematic representation of ZEISS evo SEM18, SEM instrument

3.2.5 Energy Dispersive X-ray Spectroscopy (EDS)

Energy Dispersive X-ray Spectroscopy, commonly known as EDS or EDX, is a technique used to identify which elements are present in a material and in what amounts. It is used alongside SEM for surface and elemental analysis.

When a high-energy electron beam strikes the sample's surface, it excites the atoms by knocking inner-shell electrons out of place. As the atoms stabilize by filling these vacancies with outer-shell electrons, they release energy in the form of X-rays. These emitted X-rays have energies that are unique to each element like a fingerprint. EDS uses these characteristics of X-rays to determine which elements are in the sample. It can detect

elements ranging from carbon(C) to uranium(U), even when they are present in very small amounts(about 1wt%).

The system includes three main components:

1. An X-ray detector captures the X-rays emitted from the sample.
2. A Pulse processor converts these into voltage signals.
3. A Computer records and processes the signals, displaying them as a spectrum or histogram.

The spectrum plots the energy of the detected X-rays on the x-axis and their frequency on the y-axis. Peaks in the spectrum reveal which elements are present and how much of each is there.

3.2.6 High-Resolution Transmission Electron Microscopy (HRTEM)

High-resolution Transmission Electron Microscopy, commonly known as HRTEM, is a powerful technique used to observe the internal structure of materials at the atomic or near-atomic scale. HRTEM can reveal the arrangement of atoms, crystal defects, and lattice fringes. It has extremely high resolution, often below 0.1 nanometres.

In this method, a very thin sample-often less than 100 nanometers thick, is bombarded with a beam of high-energy electrons, accelerated between 100-300 keV. As these electrons pass through the sample, they interact with the internal atomic structure, and the resulting transmitted electrons are used to form a highly magnified image on a detector.

The contrast in HRTEM image is a result of differences in electron density and atomic number, and the fringes observed often correspond to the spacing between atomic planes in the crystal lattice [27]. These fringes are used to determine interplanar spacing and crystal orientation, often supplementing XRD or SAED (selected Area Electron Diffraction) data. The instrument used is shown in figure 3.14.

Fig. 3.14 HRTEM Instrument JEM-2100F

3.2.7 UV-Vis Spectroscopy

UV-Vis spectroscopy is an ultraviolet and visible spectroscopy that examines a material's chemical composition, bandgap, and absorption behavior. we can conclude the amount of light absorbed by the sample with the help of this spectroscopy. A sample is kept free of light transmission in this technique and the computer gives spectra by gathering the light from it.

If we incident light of intensity $I_{0,}$ we get transmitted light of intensity I_t after passing through the sample. We get transmittance by the ratio of I_t/I_0. It's shown as percentages T%. Absorbance (A) can be calculated by following the equation-

$$A = -\log(T\% / 100) \qquad \text{eq. (3.1)}$$

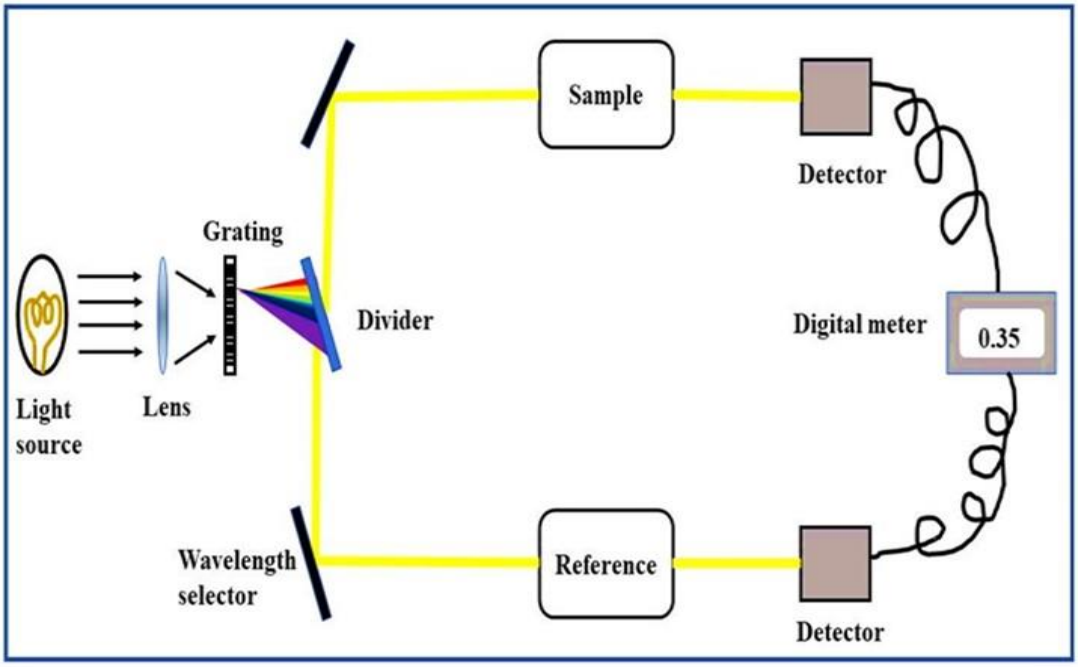

Fig. 3.15 Ray diagram of a double-beam spectrophotometer

It is a double-beam instrument made of a light source, a monochromator, two detectors, a sample cuvette, and a reference holder. There is a half mirror that divides the incoming ray into two components. Two rays pass through a reference after passing through the sample. The ray diagram of the double-beam spectrophotometer is shown in Fig. 3.15. Absorbance is calculated by the difference between the two recorded transmitted lights.

JASCO V-670 spectrophotometer (Fig. 3.16) is used to determine the absorption spectra of all the samples at room temperature. The monochromator is made of two gratings with 300 grooves per nm for NIR and 1200 grooves per nm for UV-Vis that are automatically switched. A deuterium lamp was used as the visible light source and a tungsten-halogen lamp was used for UV light. Only one lamp is turned on at a time so that there's no interference with the light. For the UV-Vis region, a Peltier-cooled PbS detector and a PMT detector are used. Gratings and detectors are automatically swapped within the wavelength range selected by the user [28,29].

Fig. 3.16 JASCO V-670, UV-Vis-NIR spectrophotometer

3.2.8 Photoluminescence Spectroscopy

Photoluminescence spectroscopy is an optical technique to figure out a material's electronic structure. This is a non-destructive method, in which the sample is excited and absorbs high-energy light. electrons come back to the ground state of the material from the excited state when excitations are diminished. Photoluminescence refers to the emission of light with a definite energy during radiative relaxation.

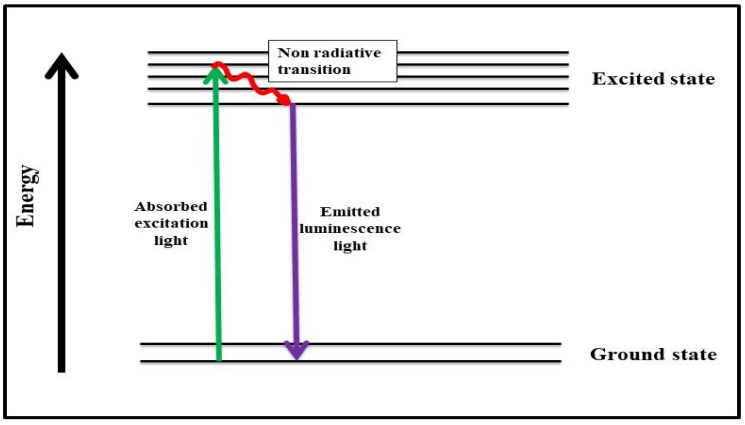

Fig. 3.17 Energy level diagram for electronic transition

Photoluminescence is of two types of fluorescence and phosphorescence. Fluorescence is stated as relaxation that happens for a very short time duration of 10^{-8} to 10^{-5} seconds. Phosphorescence refers to the relaxation over a relatively extended time. Photoluminescence's spectral content and intensity give various information about material properties directly. The above energy level diagram explains the working of photoluminescence well.

At room temperature electron is at the ground state. Electrons take energy from photons and are excited to an unstable higher excitation state from the ground state. That excitation state consists of many vibrational states. The excited electron loses some energy due to molecular transitions, so it suffers a non-radiative downward transition from a high vibrational state to a lower vibrational state. Electron travels from this lower vibrational energy level to the ground state energy level by releasing a photon with energy $E=h\upsilon$, which is the same as the energy difference between the two synchronized energy levels. Photoluminescence signifies radiation that releases visible light photons. The energy level diagram is shown in Fig. 3.17.

JASCO FP 8200 spectrofluorometer (Fig. 3.18) is used to examine the emission spectra of the prepared samples. The fluorometer consists of an excitation source, a sample cuvette, and a fluorescence detector. The excitation source of this spectrofluorometer is a shielded Xenon lamp having a wavelength range of 200-750 nm. This broadband radiation goes through a monochromator, which allows radiation of only one particular wavelength to pass. Fluorescence that is spread by an additional monochromator is identified by a photomultiplier tube. The most frequent radiative transition takes place between the conduction band and valence band of a semiconductor. The energy difference between them is known as the energy bandgap. Through photoluminescence investigation and fundamental mechanics, we can understand the recombination mechanism. This analysis can expose specific flaws or impurities within the sample [30,31].

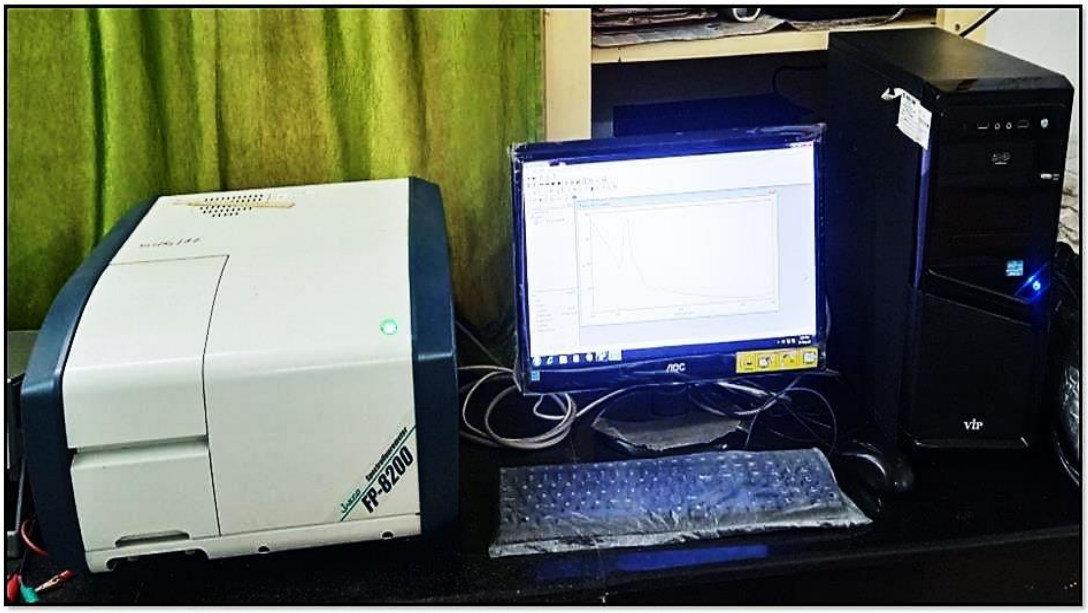

Fig. 3.18 JASCO FP-8200 Spectrofluorometer

Chapter- 4

Results and Discussion

This chapter consists of an analysis of different results obtained from different characterization techniques.

4.1 DTA study

The prepared sample was subjected to DTA analysis, which is analysis is shown in Fig. 4.1. From the figure, it is observed that the DTA curve consists of both exothermic and endothermic curves. Endothermic reactions occur at a temperature of 393.6°, corresponding to the glass transition temperature T_g. Similarly, the exothermic reaction occurs at a temperature of 623.5°C, which is considered as crystallization temperature T_c[11]. Both temperatures are critical in facilitating the formation of CuO/TiO_2 quantum dots. The synthesized glass sample undergoes heat treatment within the temperature range between Tg and Tc to promote nucleation and subsequent growth of the quantum dots [27].

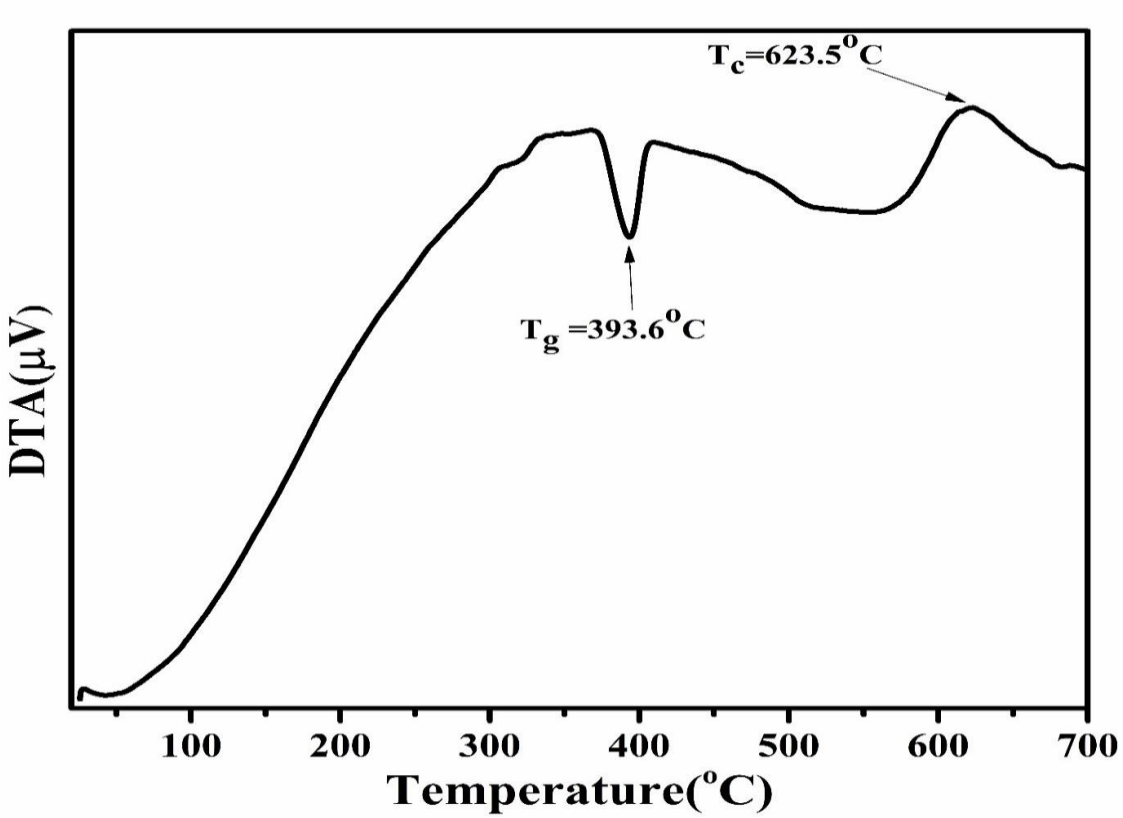

Fig 4.1 DTA plot of the synthesized sample.

4.2 Growth of Quantum Dots via Heat Treatment

The glass transition temperature (Tg) and crystallization temperature (Tc) were determined from the Differential Thermal Analysis (DTA) curve. The synthesized glass was then sectioned into five equal parts using a diamond cutter, and each piece was labeled as CTG_0, CTG_1, CTG_2, CTG_3, and CTG_4. Except for CTG_0, all samples were subjected to a carefully optimized single-step heat treatment to facilitate quantum dot growth. A suitable temperature falling between Tg and Tc was selected, with the optimized heat treatment temperature set at 500 °C. The samples were then thermally treated for varying durations as detailed in Table 4.1.

Sample ID	Description
CTG_0	**As made glass**
CTG_1	**Glass heated at 500°C for 4hr**
CTG_2	**Glass heated at 500°C for 6hr**
CTG_3	**Glass heated at 500°C for 8hr**
CTG_4	**Glass heated at 500°C for 10hr**

Table 4.1 Heat treatment for synthesized samples

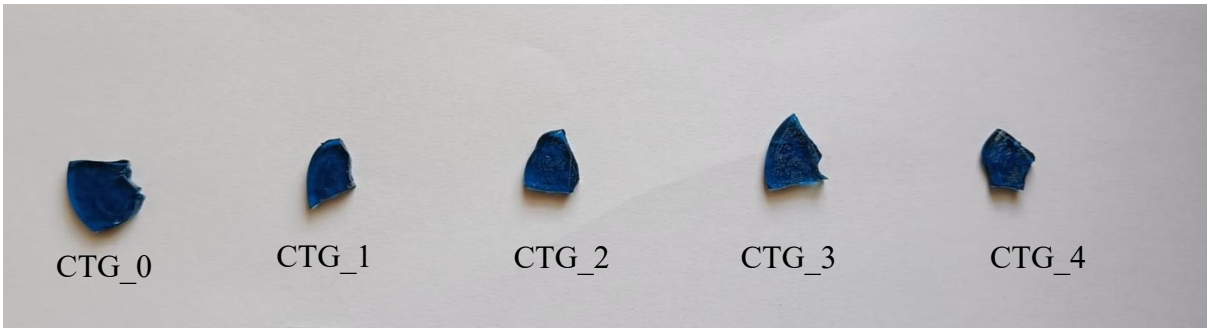

Fig. 4.2 samples after heat treatment

The glass formed was dark blue, and the colour remained the same even after the heat treatment. The development of CuO/TiO_2 quantum dots results from nucleation and subsequent growth triggered by thermal energy during heat treatment. The size of the resulting quantum dots is influenced by the treatment temperature [32].

4.3 X-Ray Diffraction (XRD) Analysis

X-ray diffraction analysis was done to find the phase formation of CuO/TiO_2 quantum dots embedded in the sodium borosilicate glass matrix. Fig. 4.3 displays the XRD patterns of the as-prepared glass (CTG_0) and the sample heat-treated at 500°C for 10 hours (CTG_4). The CTG_0 sample shows no distinct diffraction peaks, indicating that the glass remains amorphous in its initial state. After thermal treatment, the CTG_4 exhibits a weak diffraction peak, suggesting the onset of crystallite formation within the glass due to heat treatment.

In the CTG_4 sample, the peak corresponding to (101) is observed at 2θ angles of 28.19°. This peak aligns with the standard JCPDS file No. 21-1272 for anatase TiO_2 [33], confirming the presence of crystalline phases. Despite this, the overall peak intensity remains low, likely due to the limited concentration of semiconductor nanocrystals and the dominant amorphous nature of the glass matrix.

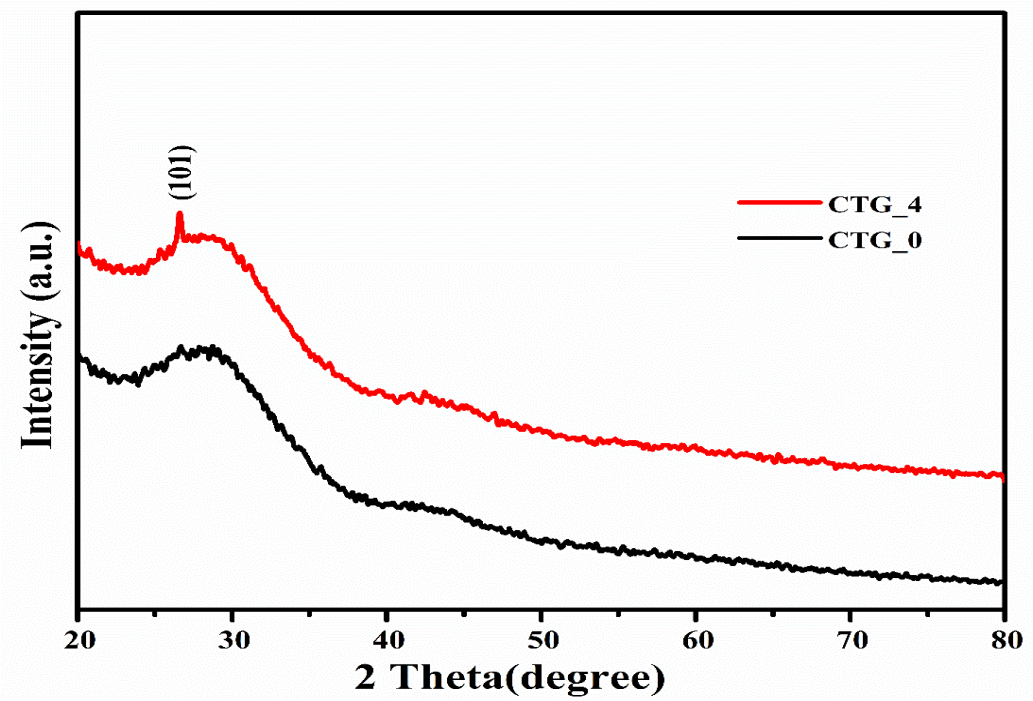

Fig. 4.3 XRD spectra for the synthesized sample.

4.4 Raman Analysis

Raman spectroscopy is known for its sensitivity to crystal structure, doping levels, and lattice imperfections. The structure of prepared nanoparticles is additionally confirmed

through Raman analysis, using a laser of 532 nm at room temperature (Fig. 4.4). According to factor group analysis, all the Raman bands belong to six Raman active modes ($2A_g$, + A_{1g},+ B_g +$2B_{1g}$ + $2E_g$) [34]. All these eight Raman active modes were observed, and the leading peak is at 209 cm^{-1} which approves the anatase phase of TiO_2. The other anatase peaks observed at 643 cm^{-1} and 551 cm^{-1} correspond to different vibrational modes. Specifically, they represent the symmetric bending vibration (B_{1g}), anti-symmetric bending vibration (A_{1g}), and symmetric stretching (E_g) of the O-Ti-O bond [35].

Peaks for CuO were found at 276 cm^{-1}, 298 cm^{-1},340 $cm^{-1,}$ and 443 cm^{-1} [35]. From the spectra, it is observed that as the thermal treatment temperature increases, peaks intensity decreases. The decrease in Raman peak intensity with heat treatment is most commonly due to crystalline phase dissolution into the glass, phase transformation, or loss of nanostructured order, all of which diminish the Raman-active vibrational modes.

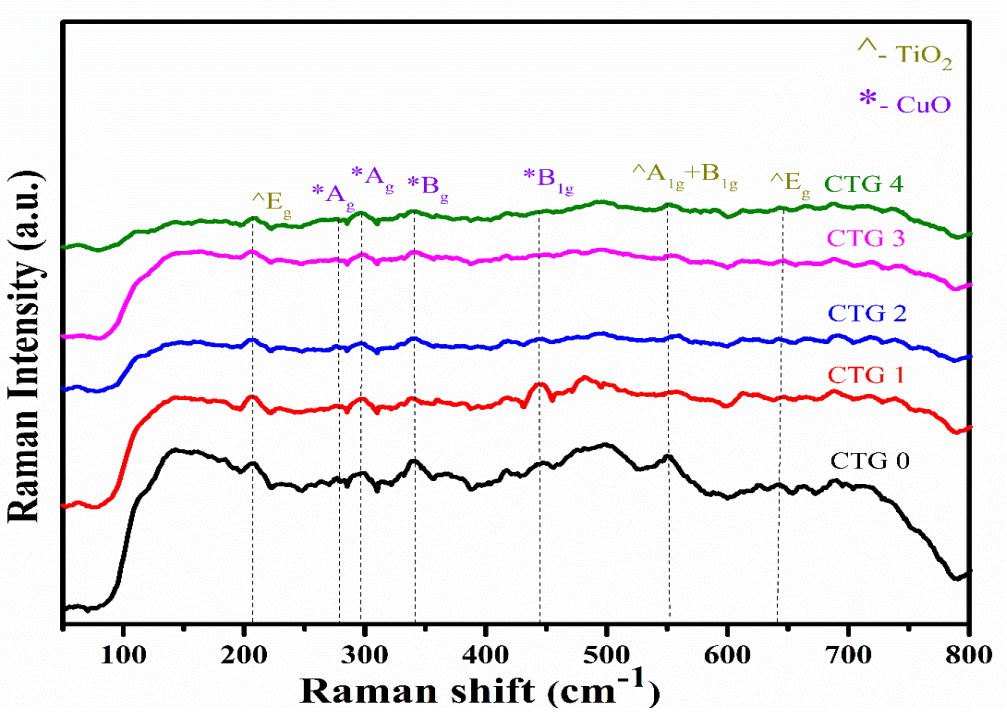

Fig. 4.4 Raman spectra for the synthesized sample

4.5 FTIR Analysis

Fourier Transform infrared spectroscopy serves as a powerful technique for investigating the structural framework and functional groups of prepared materials. Fig. 4.5 displays the FTIR spectra of the prepared glass samples, highlighting the vibrational modes associated with bending and stretching of bonds formed between various inorganic constituents within the glass matrix. The observed band positions and their corresponding vibrational assignments are in Table 4.2.

A noticeable trend in the spectra is the gradual shift of absorption bands towards higher wavenumber with increasing heat treatment duration. This shift is primarily influenced by the presence of alkali oxides such as Na_2O and K_2O in the glass composition. Upon heating beyond the glass transition temperature, these alkali components promote structural recognition of the glass network and increase the mobility of free ionic species. Thermal energy softens the glass structure, enabling ions to migrate and occupy interstitial sites.

Simultaneously, the thermal environment facilitates the nucleation and growth of CuO/TiO_2 quantum dots via the Ostwald ripening mechanism. These QDs tend to form in proximity to the alkali ions within the interstitial regions, resulting in local expansion of the glass network. Consequently, the combined effect of alkali ion diffusion and QD growth results as a spectral shift toward higher energy in the FTIR spectrum. It becomes more pronounced with longer heating durations and larger QD sizes [36].

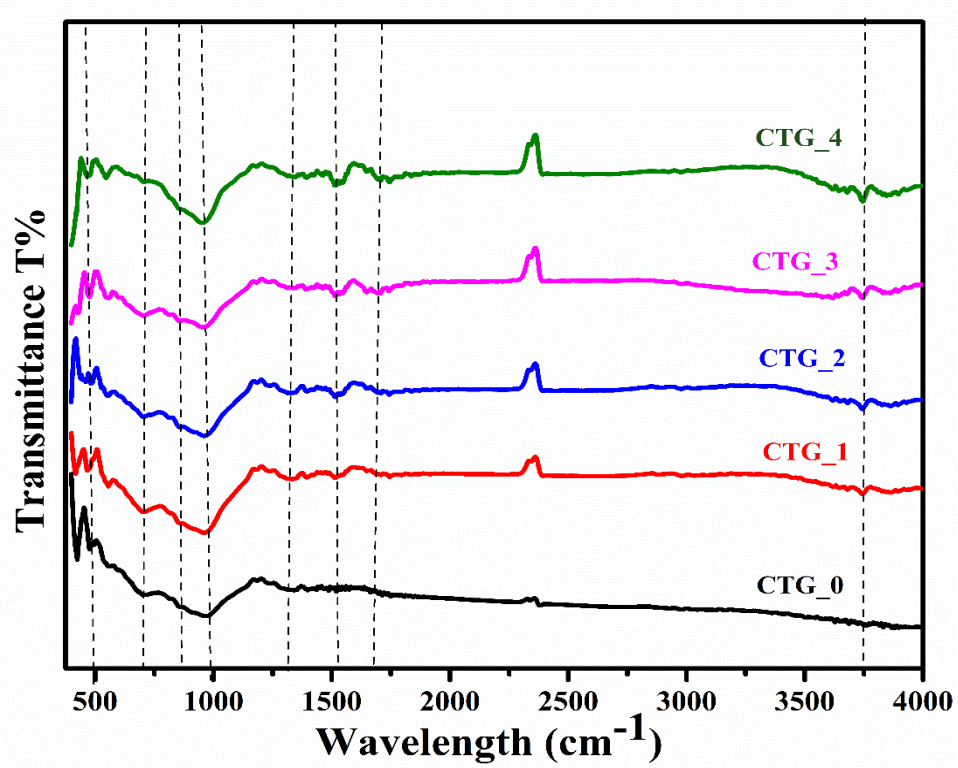

Fig. 4.5 FTIR spectra for the synthesized sample

FTIR peak position for glass samples for different heating time					
CTG_0	**CTG_1**	**CTG_2**	**CTG_3**	**CTG_4**	**Description**
476	466	460	476	472	Bending vibration of Si-O-Si link
705	704	702	704	707	Bending of B-O-B linkage
862	862	862	862	862	Stretching of BO_4
968	960	960	956	950	Stretching of B-O-Si linkage
1325	1328	1328	1328	1340	Asymmetric vibration of B-O
-	1512	1516	1512	1512	Asymmetric vibration of BO_3
3747	3745	3743	3743	3743	O─H stretching vibrations

Table 4.2. FTIR peaks shifting with description

4.6 SEM and EDS Analysis

The surface morphology of the glass powder was examined using scanning electron microscopy (SEM), as shown in Fig. 4.6. The glass sample was mechanically ground for two different durations- 0 hours and 10 hours, referred to as CTG_0 and CTG_4, respectively. This reveals the irregular, stone-like particles typical of ground glass. Based

on particle size distribution histograms (Fig. (e) & (f)), the average particle sizes for CTG_0 and CTG_4 were estimated to be approximately 5.49 and 3.28 μm, respectively.

Field emission scanning electron microscopy (FESEM) images provide further insight into the morphology of samples. These micrographs confirm the presence of uniformly distributed grains, indicating the formation of CuO/TiO_2 nanocrystals. Over time, these nanocrystals tend to cluster due to agglomeration, forming larger assemblies of quantum dots through the Ostwald ripening mechanism. Heat treatment softens the glass matrix, allowing the nanoparticles to migrate into interstitial regions where they coalesce into clusters [11]. This softening is attributed to increased thermal vibrations within the matrix during annealing.

Furthermore, energy-dispersive X-ray spectroscopy (EDS) analysis of the CTG_4 in figure 4.6 (c) & (d) confirmed the presence of elements consisting of materials used for glass synthesis and incorporation of target components during the fabrication process [37].

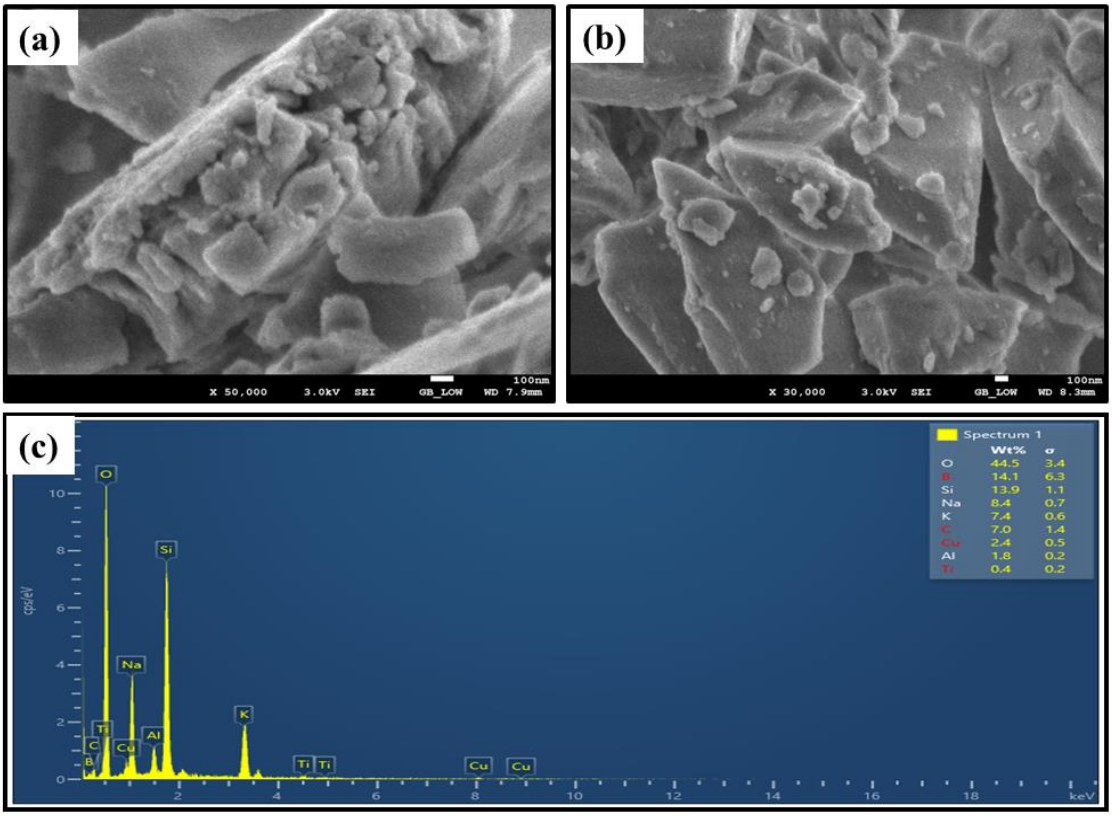
(a)
X 50,000 3.0kV SEI GB_LOW WD 7.9mm
100nm
(b)
X 30,000 3.0kV SEI GB_LOW WD 8.3mm
100nm
(c)
Spectrum 1
Wt% σ
O 44.5 3.4
B 14.1 6.3
Si 13.9 1.1
Na 8.4 0.7
K 7.4 0.6
C 7.0 1.4
Cu 2.4 0.5
Al 1.8 0.2
Ti 0.4 0.2
O
Si
Na
K
Ti
C
B
Cu
Al
Ti Ti
Cu Cu
cps/eV
keV

(d)

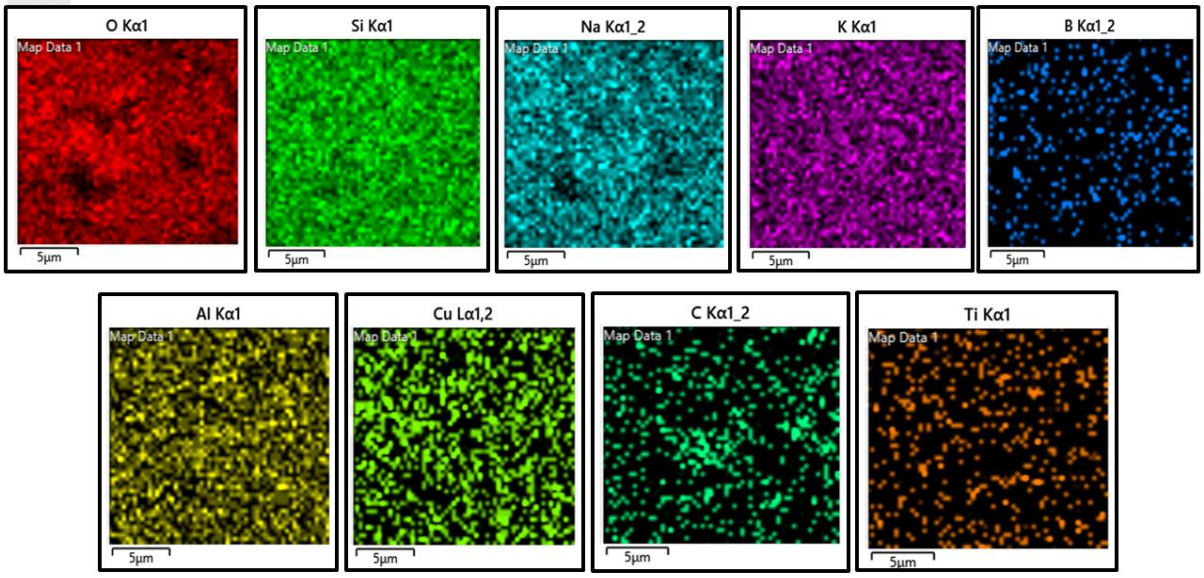
O Kα1
Si Kα1
Na Kα1_2
K Kα1
B Kα1_2
Al Kα1
Cu Lα1,2
C Kα1_2
Ti Kα1
Map Data 1
5µm

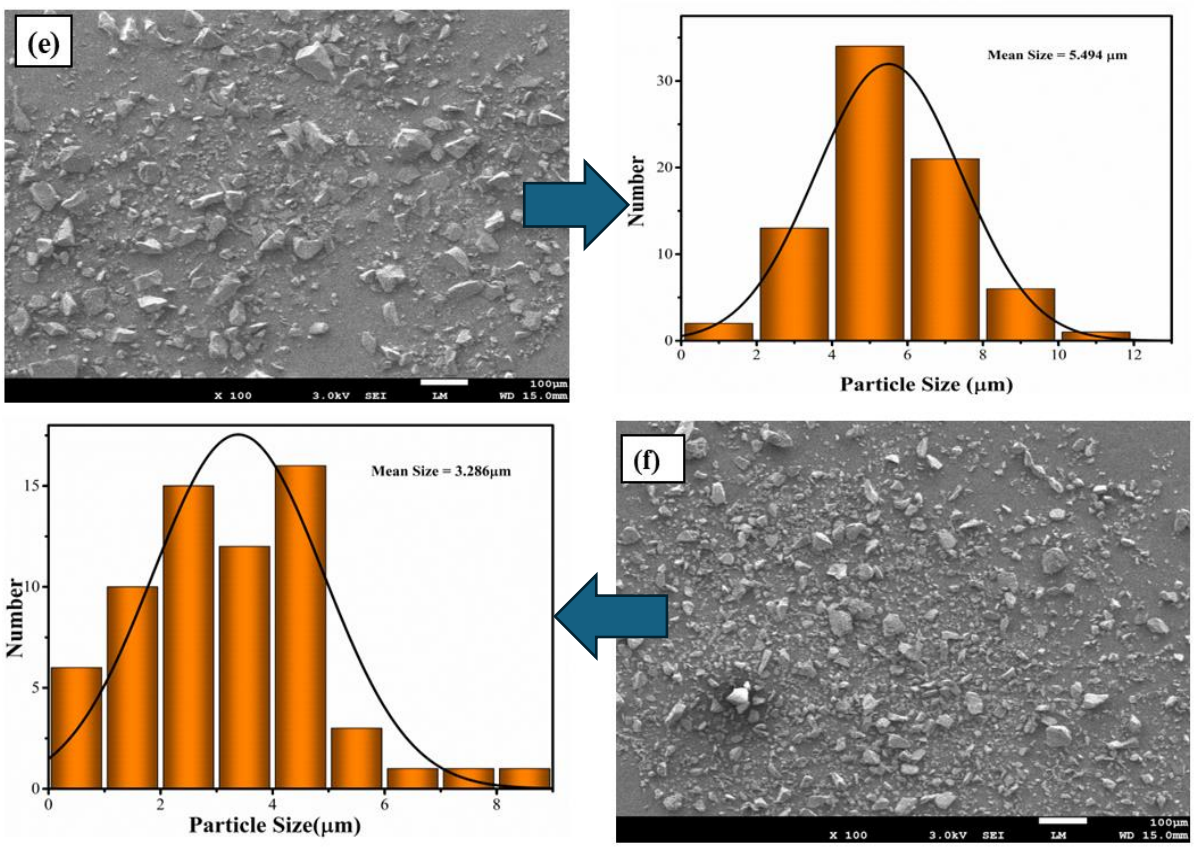

Fig. 4.6 (a) FESEM image of CTG_0, (b)FESEM image of CTG_4 (c) EDS spectra of CTG_4 (d) elemental mapping of CTG_4 (e) histogram of CTG_0 (f)histogram of CTG_4.

4.7 HRTEM Analysis

High resolution transmission electron microscopy (HRTEM) was used to study the microstructural characteristics of glass samples annealed at 500°C for 10 hr. The CTG_4 sample was used due to its finer particle size. Fig. 4.7(a) displays the HRTEM micrographs, revealing uniformly distributed, spherical dark regions corresponding to CuO/TiO_2 quantum dots (QDs). The size distribution of these QDs is determined from the histogram (Fig. 4.7 (b)), indicating an average diameter of approximately 2.4 nm.

Further examination of the HRTEM images, as shown in Fig. 4.7c, reveals distinct lattice fringes with interplanar spacing of 0.246 nm and 0.334 nm. These spacings correspond to the (002) plane of CuO and the (101) plane of anatase TiO_2, respectively, confirming the presence of both crystalline phases within the glass matrix. The selected area electron diffraction (SAED) pattern, presented in the inset of Fig. 4.7(d), exhibits well-defined

diffraction spots, substantiating the crystalline nature of the embedded QDs. These observations align with standard reference data from JCPDS cards 45-0937 for CuO and 21-1272 for anatase TiO_2 [38].

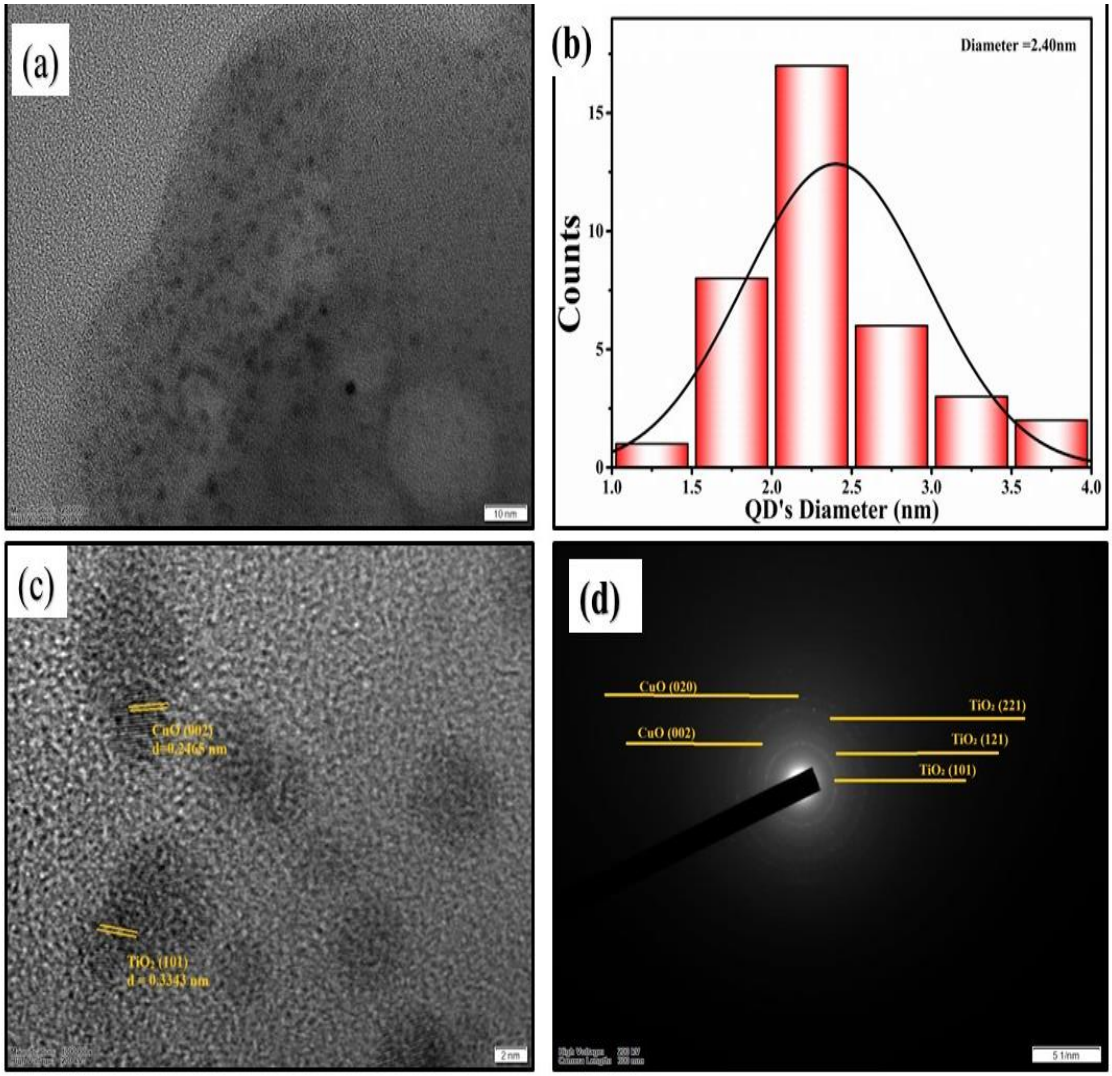

Fig. 4.7 (a) HRTEM image of CTG_4, (b) histogram of QD size in CTG_4, (c) d-spacing in CTG_4, (d) SAED pattern

4.8 UV-Visible absorption spectroscopy

UV-Vis spectra were measured to analyze the optical properties of all prepared samples, which are shown in Fig. 4.8. The optical absorption characteristics of the CuO/TiO_2 photocatalysts were studied within the wavelength range of 300 to 700 nm [39]. The absorption spectra reveal that, with an increase in heat treatment duration at a constant temperature across different glass samples, the optical cut-off wavelength shifts toward

longer wavelengths—a phenomenon known as red shift. This shift is likely attributed to the growth in the size of the semiconductor nanocrystals.

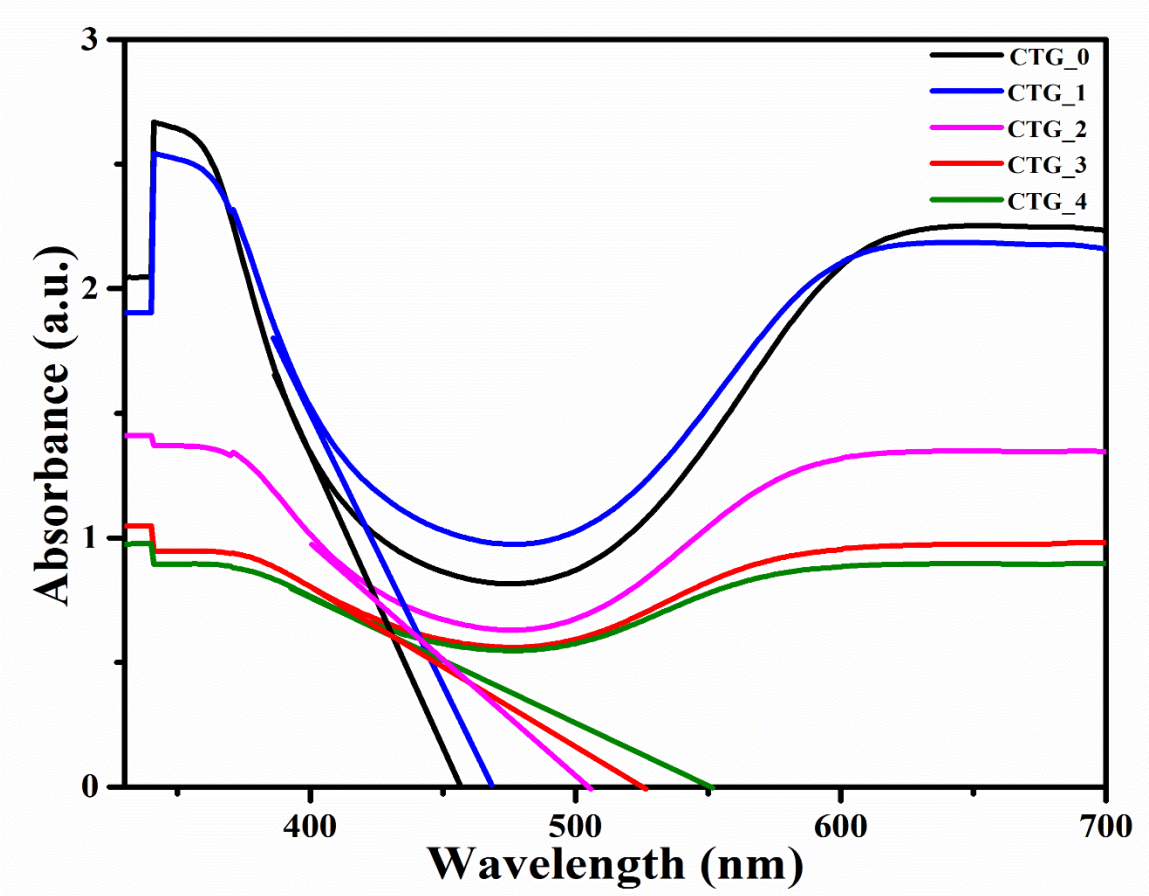

Fig. 4.8 UV-Vis plot for all samples

Band gap energy was calculated by Tauc's plot with the help of the following equation:

$$(\alpha h\upsilon) = A\,(h\upsilon - E_g)^n \qquad \text{eq. (4.2)}$$

where E_g signifies the energy band gap, $h\upsilon$ denotes the energy of the photon, α stands for the absorption coefficient, A is a constant, and the value of n varies depending on the nature of transitions: n=1/2 corresponds to a direct allowed transition, while n = 2 indicates an indirect allowed transition [20]. Tauc's plot for all synthesized samples is shown in Fig. 4.9.

The calculated band gap values can be found by determining the intercept of the tangent to the X-axis and are depicted in Table 4.3. The presence of CuO/TiO_2 lattice improves the visible light absorption, showing a decrease in energy bandgap. The reduction in energy band gap values may be due to the creation of defect energy levels between the CB and VB of TiO_2. The table shows that the optical energy band gap for CTG_0 is 2.99

eV, and it decreases with an increase in annealing time. The decrease in energy band gap confirms that the size of quantum dots increases with annealing time.

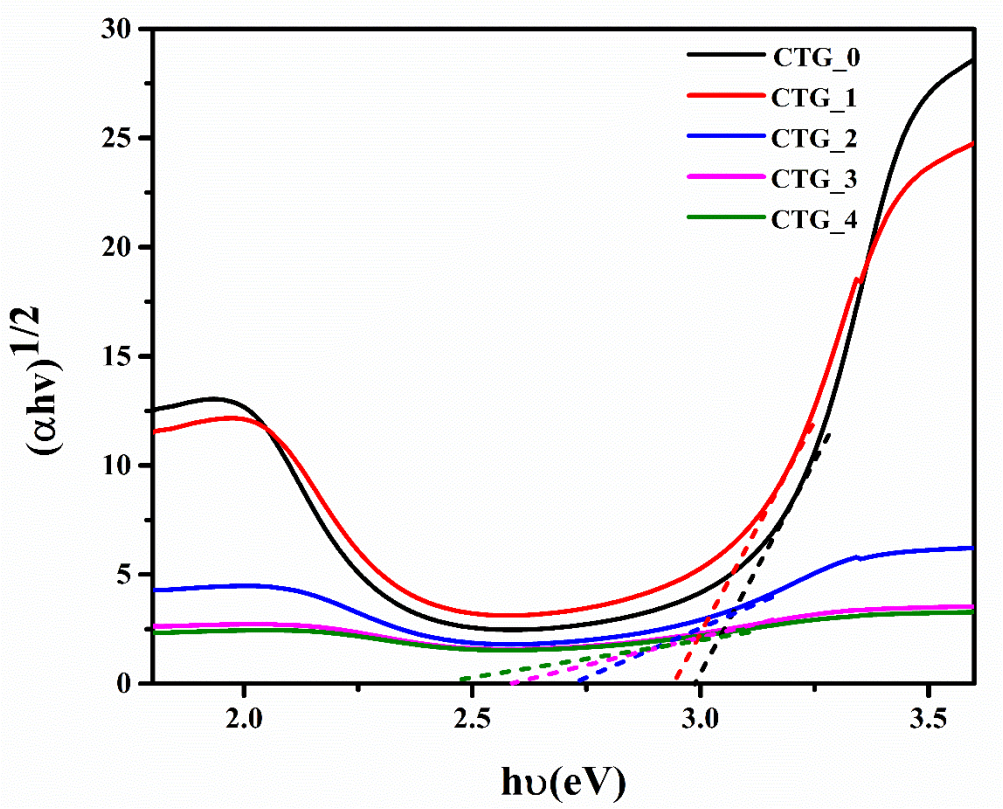

Fig. 4.9 Tauc's plot for all samples.

Sample name	Optical band gap(eV)
CTG_0	2.99
CTG_1	2.94
CTG_2	2.73
CTG_3	2.58
CTG_4	2.47

Table 4.3 Optical band gap of all samples.

4.9 Photoluminescence

Photoluminescence spectroscopy (PL) is a practical method for probing the electronic structure of nanomaterials, the behaviour of the photo-excited electrons in semiconductors, and the rate of recombination. The PL spectra for all the measured samples are shown in Figure 4.9 It is observed that PL emission spectra of CuO/TiO_2 excited at 350 nm at room temperature give peaks at 412, 433, and 459 nm.

According to Fig. 4.10, PL intensity first decreases and then increases with increasing annealing time. The electron-hole pair recombination is the reason for the photoluminescence spectra. Photocatalyst CTG_4 shows the lowest PL intensity. The lower PL intensity shows a lower recombination rate of electron-hole pairs that enhances the Photocatalytic activity of the sample. This is due to the formation of new trap sites on the surface. Due to low electron-hole pair recombination, more electrons and holes will be available for oxidation and reduction reactions, respectively, so more dye degradation [39,40].

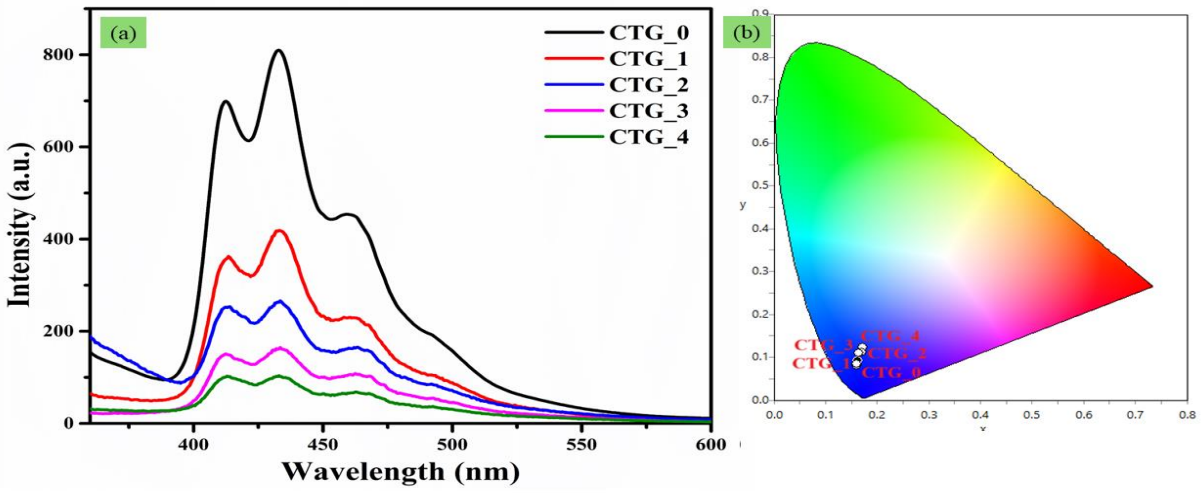

Fig. 4.10(a)PL spectra for all prepared samples & (b)CIE plot for all synthesized samples

Figure 4.10 presents the CIE chromaticity diagram for all glass samples (coordinates in Table 3). Notably, the CTG_4 specimen, after a 10 h heat treatment, plots at x = 0.17 and y = 0.12 and exhibits the strongest emission intensity in the deep blue region.

Sample ID	X- coordinate	Y- coordinate
CTG_0	0.1588	0.0804
CTG_1	0.1597	0.0854
CTG_2	0.1699	0.1114
CTG_3	0.1637	0.1094
CTG_4	0.1714	0.1230

Table no. 4.4 Coordinates of CIE plot for all samples.

CHAPTER 5

DEGRADATION OF ORGANIC DYE

5.1 Experiment

The photocatalytic activity of CuO/TiO_2 QDs contained in glass was carried out for Indigo carmine (IC) as an organic pollutant in the presence of Sunlight. For the photocatalysis study, a 100 mL, 5 ppm aqueous solution of IC dye was prepared. The reaction was carried out with the catalyst in powder form, i.e., glass powder, as well as for the catalyst in the solid form, i.e., glass separately. For powder catalyst, 0.05 gm glass powder as a catalyst was added to 100 mL of aqueous solution of IC dye and for the glass catalyst whole glass which was heat treated was added in the 100 ml aqueous solution of IC dye and both were stirred in a dark environment for 30 min to ensure the uniform dispersion and adsorption-desorption equilibrium between the catalyst surface and the dye molecules. This whole set-up was then brought into the sunlight and stirred for 5 hours, and after that, at every interval of 1h, 3-4 ml solution was collected, and the absorption spectra were noted to determine the remaining concentration of dye with an increase in irradiation time. Under an average energy density of solar radiation of about 1044 W/m^2, the rate of reaction and degradation efficiency were studied by absorption spectra using the JASCO V-670 spectrophotometer.

5.2 Result

Synthesized CuO/TiO_2 QDs were examined for the degradation of Indigo Carmine dye via two different forms of catalyst. As for degradation performance, a 5 ppm I dye solution was prepared. 50 mg of powder photocatalyst and glass as solid catalyst were added, individually, in two different beakers containing dye. Absorption spectra of degraded IC dye solution with the most efficient photocatalyst CTG_4 are shown in Fig. 5.1 and Fig. 5.2. The peak intensity of IC dye at nm decreases with time, which shows a decrease in the concentration of dye. Under dark conditions, absorption spectra are reduced because of the adsorption-desorption of dye particles on the photocatalyst surface [20]. Afterward, absorption of dye decreases extremely when checked under visible light irradiation and completely disappears within 5 hours.

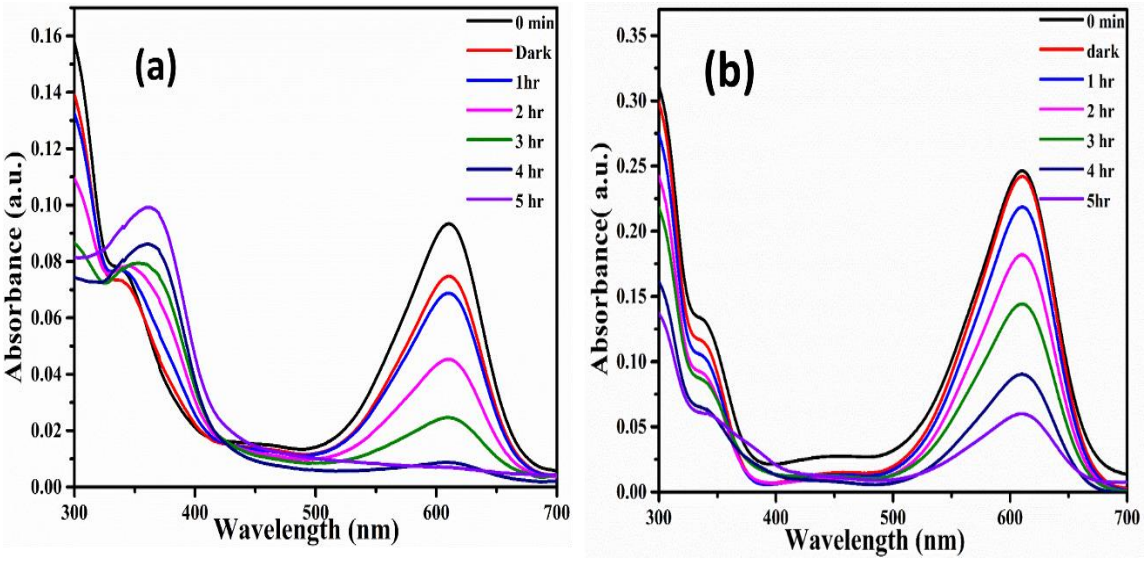

Fig 5.1 Absorption spectra of (a)glass sample(solid catalyst),(b) glass powder (powder catalyst)

The Beer-Lambert law was used to determine dye concentration,

$$C = \frac{A}{\varepsilon l} \qquad \text{eq.5.1}$$

Where A shows absorbance, C is the concentration of the solution, ε represents the molar absorption coefficient, and l is the optical path. The degradation efficiency of the sample was calculated by following the formula,

$$\text{Efficiency (\%)} = (1 - \frac{C}{C_0}) \text{ X } 100 \qquad \text{eq. 5.2}$$

C_0 is the initial concentration, and C is the concentration at time t [41,42].

The degradation of IC dye for both photocatalysts was examined in the same atmosphere. Fig. 5.3 depicts a plot for the relative concentration of dye with irradiation time. The concentration of dye decreased drastically with the addition of a photocatalyst under sunlight irradiation. The degradation efficiency for both photocatalysts was determined and tabulated in Table 5.1.

.

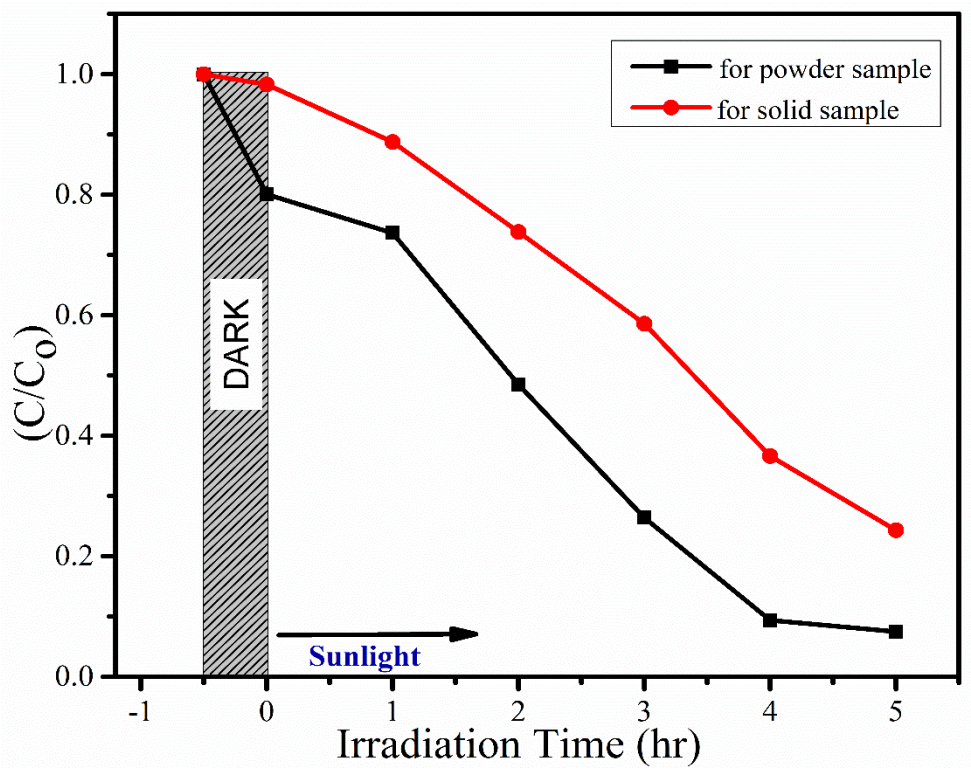

Fig. 5.2 Relative concentration of IC dye with irradiation time

The absorption spectra show that the heat-treated CuO/TiO_2 shows excellent photocatalytic activity. It is observed that dye concentration is decreasing with irradiation time. The decline of concentration in the powder sample is much faster than in the solid sample. This might be due to the larger surface area present in the powder form, and the reaction happens on the surface of the sample [43].

The degradation of Indigo Carmine in the presence of a photocatalyst follows pseudo-first-order reaction kinetics.

$$\ln(\frac{C_0}{C}) = kt \qquad \text{eq. 5.3}$$

where C_0 and C are initial and time-varying concentrations, k shows the reaction rate, and t represents the irradiation time[44].

The plot of $\ln(C_0/C)$ against time is shown in fig. 5.3. The linear fitting of the plot of $\ln(C_0/C)$ against time was used to determine reaction rate k and tabulated in Table 5.1.

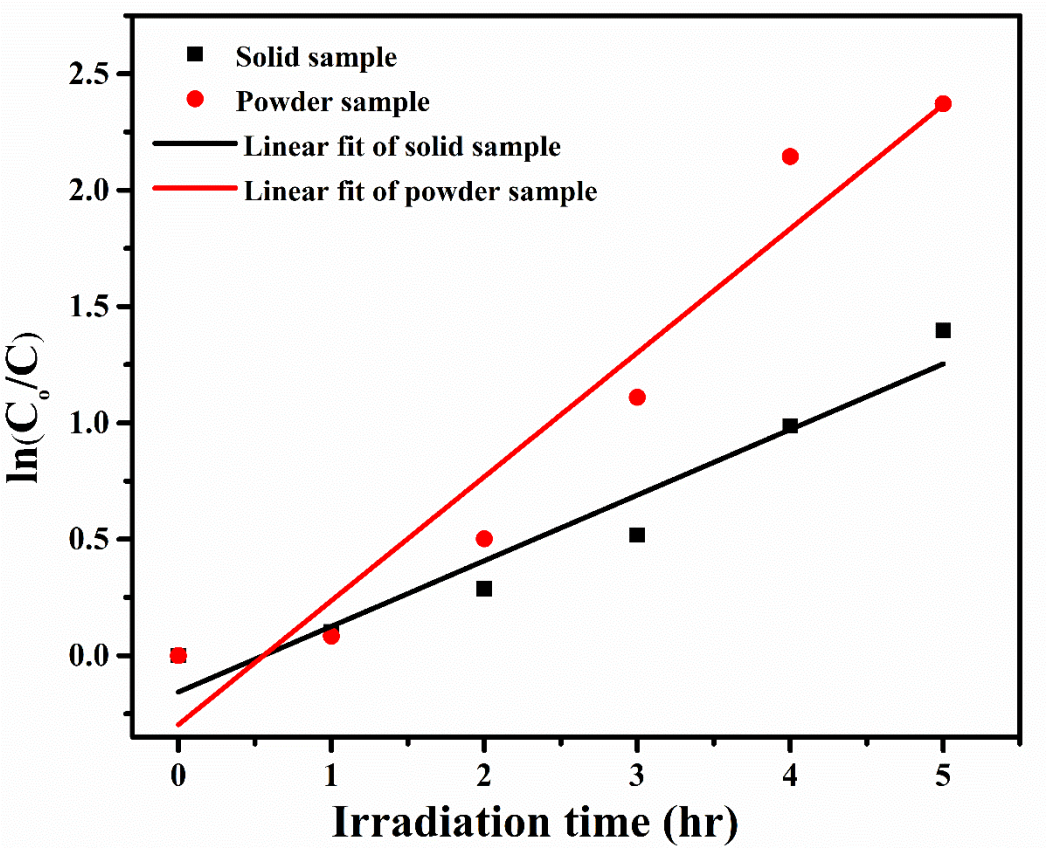

Fig. 5.3 plot of ln(C₀/C) against irradiation time

Sample	Degradation Efficiency for 5 hr.	Reaction Rate/hour
Glass powder(powder sample)	92.52 %	0.53
Glass (solid sample)	75.68 %	0.28

Table 5.1 Reaction rate and efficiency of both samples.

5.3 Reusability

The reusability and durability of photocatalysts are crucial parameters for practical applications. For the stability test, the photocatalyst powders (powder sample) were collected via centrifugation after the degradation of IC in the solution. These powders were then cleaned with distilled water to eliminate any remaining IC and dried before being used in another photocatalytic reaction. For the glass sample (solid sample), it was cleaned

with distilled water after degradation of IC in solution and used as it was for the next cycle. This procedure was repeated four times. Fig. 5.5((a) & (b)) shows that the CTG_4 photocatalyst was utilized for four cycles of IC photodegradation to evaluate the stability and recyclability of the photocatalyst. It can be observed from the figure that the removal efficiency was largely maintained after four cycles for the glass powder sample, and for the glass sample, it remained the same throughout the cycles. It was, indicating the good stability of the prepared photocatalyst. The slight decrease in efficiency of the powder sample after each cycle may be due to the formation of by-products, which accumulated on the surface and blocked the active surface of the photocatalyst, which in turn reduced efficiency, whereas no accumulation was observed on the surface of the glass sample.

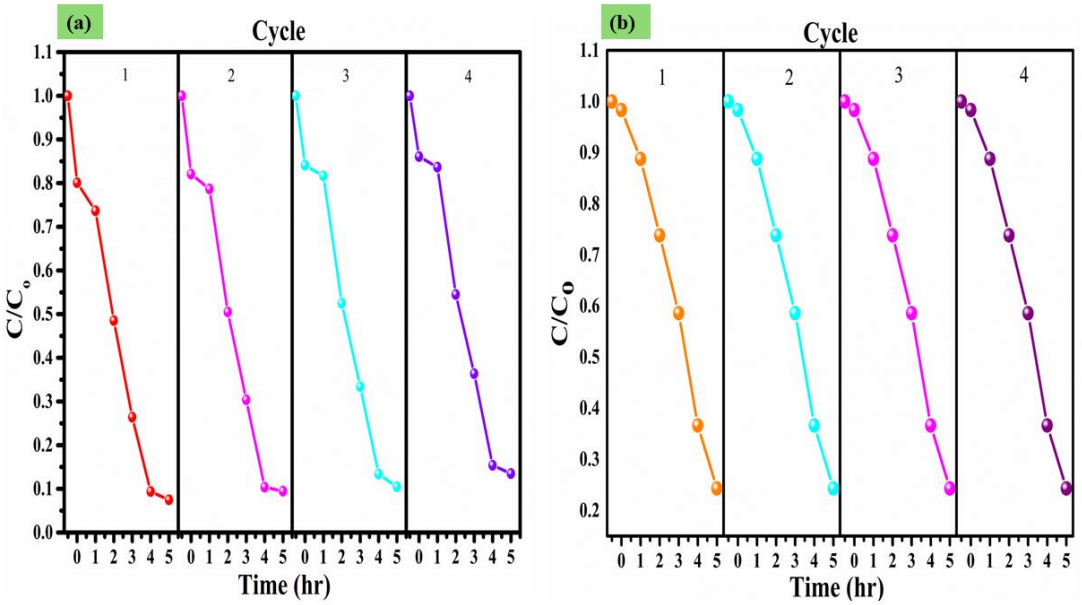

Fig. 5.4 reusability of (a) glass powder (powder sample)&(b) glass sample (solid sample)

5.4 Mechanism

The photocatalytic mechanism of Indigo Carmine (IC) dye under sunlight is discussed, and the mechanism is depicted in Fig. 5.5.

The potential edge of CB and VB for the semiconductor was calculated using equations of Mulliken's electronegativity.

$$E_{(CB)} = \chi - E_C - 0.5 * E_g \qquad \text{eq 5.4}$$

$$E_{(VB)} = E_g + E_{(CB)} \qquad \text{eq 5.5}$$

The electronegativity (χ) of a semiconductor is typically determined by taking the geometric mean of the electronegativities of its constituent atoms. The energy level of a free electron on the hydrogen scale, denoted as Ec, is commonly taken to be 4.5 eV. The energy band gap (Eg) of the semiconductor is also a key factor in determining its electronic properties. For titanium dioxide (TiO_2), the conduction band (CB) and valence band (VB) edge potentials are approximately -0.29 eV and 2.91 eV, respectively. In comparison, for copper oxide (CuO), these values are around 0.46 eV (CB) and 2.16 eV (VB). It is well established that CuO has a conduction band with a more positive potential (i.e., less negative) than that of TiO_2. Additionally, the valence band of CuO is considered less cationic in nature compared to TiO_2. Due to these band alignments, direct electron transfer from the conduction band of CuO to that of TiO_2 is not energetically favorable under sunlight irradiation.

Under sunlight irradiation, there is a possibility of electron transfer from the valence band (VB) of TiO_2 to the VB of CuO. This phenomenon is known as direct photo-induced interfacial charge transfer (IFCT). As a result of this process, a hole is left behind in the valence band of TiO_2. Repetition of this charge transfer enhances the separation of charge carriers, thereby minimizing the likelihood of electron-hole (e^-–h^+) recombination. Consequently, the system maintains a hole in TiO_2's VB and an electron in CuO's conduction band (CB). These separated charge carriers actively contribute to the photocatalytic reaction, leading to more efficient dye degradation. Therefore, the formation of a CuO/TiO_2 heterojunction and the improved charge separation facilitated by the IFCT mechanism significantly boost the overall photocatalytic performance [45].
The actual mechanism of photocatalysis is given below: -

$$CuO/TiO_2 + h\upsilon(>420nm) \rightarrow CuO(e^-_{CB} + h^+_{VB})/TiO_2$$

$$CuO(e^-_{CB} + h^+_{VB})/TiO_2 \rightarrow CuO\,(h^+_{VB})/TiO_2\,(h^+_{VB}) + CuO\,(e^-_{CB})$$

$$CuO(e^-) + O_2 \rightarrow O_2^{\bullet -} \quad (E = -0.29\ eV)$$

$$O_2^{\bullet -} + H_2O \rightarrow HO^{\bullet} + OH^-$$

$$HO^{\bullet} + H_2O \rightarrow OH^{\bullet} + H_2O_2$$

$$H_2O_2 \rightarrow 2OH^{\bullet}$$

$$OH^{\bullet} + IC\ (dye) \rightarrow CO_2 + H_2O \quad (E = 2.91\ eV)$$

$$CuO/TiO_2\ (h^{+}_{VB}) + H_2O \rightarrow OH^{\bullet} + H^{+} \quad (E = 2.16\ eV)$$

$$OH^{\bullet} + IC\ (dye) \rightarrow CO_2 + H_2O$$

Upon exposure to sunlight, electrons in the valence band (VB) of CuO become excited and transition to its conduction band (CB), leaving behind holes in the VB. Due to the relatively higher potential of CuO's conduction band compared to that of TiO_2, these excited electrons are unable to migrate to the CB of TiO_2. Nevertheless, a direct photo-induced interfacial charge transfer (IFCT) from the valence band of TiO_2 to the valence band of CuO takes place under solar irradiation. The electrons present in the CB of CuO subsequently reduce molecular oxygen to form superoxide anions ($O_2^{-}\bullet$), while the holes generated in the VB of TiO_2 oxidize water molecules to produce hydroxyl radicals (•OH). These highly reactive radicals contribute significantly to the degradation of dye pollutants by initiating the oxidative breakdown of the dye molecules.

The findings of this study indicate that glass matrices embedded with CuO/TiO_2 quantum dots serve as effective photocatalysts for dye degradation. Notably, the heat-treated glass sample in powdered form exhibits the highest degradation efficiency, which is attributed to a reduction in the material's energy band gap, thereby enhancing light absorption and charge carrier activity [46].

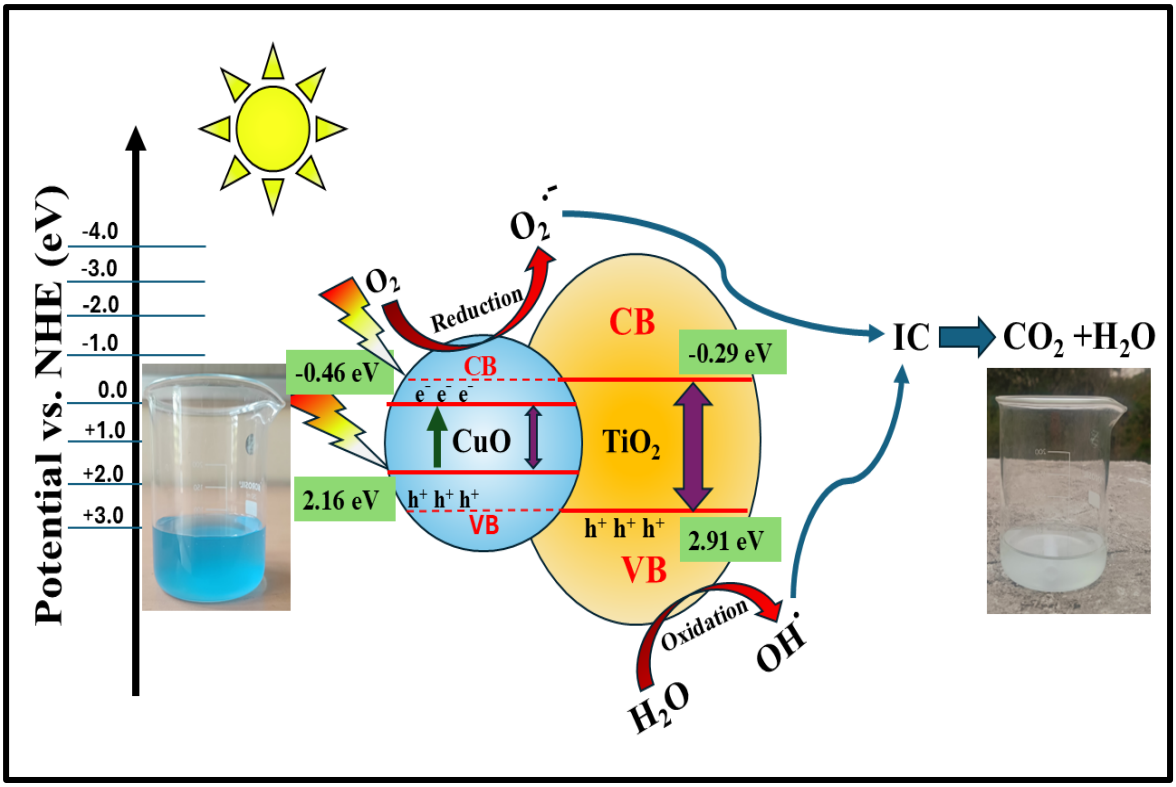

Fig. 5.5 Schematic representation of the mechanism of CuO/TiO_2 heterojunction photocatalyst for degradation of IC dye.

Chapter 6

CONCLUSION AND FUTURE SCOPE

6.1 Conclusion

Sodium borosilicate glass doped with CuO/TiO_2 was synthesized by the melt quench method. Prepared glass was heat-treated to grow CuO/ TiO2 QDs. The amorphous phase of glass was confirmed by XRD analysis. The formation of the anatase and brookite phases of TiO_2 in all the prepared samples was confirmed by XRD and Raman spectra. The SEM analysis revealed that the surface was sensitive to the heat treatment and the existence of Ti, O, and Cu, and the purity of the prepared sample was verified by EDS analysis. The FTIR analysis confirmed the presence of inorganic elements of the glass matrix. The size of the QDs was confirmed by HRTEM, and the phases of TiO_2 and CuO were also confirmed. UV-Vis spectra show that the energy band gap value decreases with increasing heat treatment. PL analysis confirms CTG_4 as the best photocatalyst, having the lowest electron-hole recombination rate. The Photocatalytic activity of 5 ppm IC dye with 50 mg photocatalyst was examined for CTG_4 sample in powder and solid form, and the highest efficiency was found to be 92.23% for the CTG_4 photocatalyst in powder form (glass powder) and 75.68 % for the CTG_4 in solid form (glass), in 5 hours.

6.2 Future Scope

1) Antimicrobial activity can be examined for prepared samples.
2) Other dyes like Methyl Blue, methyl orange, and rhodamine can be tested for photocatalytic activity using synthesized samples.
3) Self-cleaning of prepared samples can be investigated.
4) Air purification can be tested for prepared samples

References

[1] M.F. Lanjwani, M. Tuzen, M.Y. Khuhawar, T.A. Saleh, Trends in photocatalytic degradation of organic dye pollutants using nanoparticles: A review, Inorg. Chem. Commun. 159 (2024) 111613. https://doi.org/10.1016/j.inoche.2023.111613.

[2] G. Crini, Non-conventional low-cost adsorbents for dye removal: A review, Bioresour. Technol. 97 (2006) 1061–1085. https://doi.org/10.1016/j.biortech.2005.05.001.

[3] C.I. Pearce, J.R. Lloyd, J.T. Guthrie, The removal of colour from textile wastewater using whole bacterial cells: A review, Dye. Pigment. 58 (2003) 179–196. https://doi.org/10.1016/S0143-7208(03)00064-0.

[4] R. Gong, Y. Sun, J. Chen, H. Liu, C. Yang, Effect of chemical modification on dye adsorption capacity of peanut hull, Dye. Pigment. 67 (2005) 175–181. https://doi.org/10.1016/j.dyepig.2004.12.003.

[5] V.K. Gupta, Suhas, Application of low-cost adsorbents for dye removal - A review, J. Environ. Manage. 90 (2009) 2313–2342. https://doi.org/10.1016/j.jenvman.2008.11.017.

[6] S. Chen, J. Zhang, C. Zhang, Q. Yue, Y. Li, C. Li, Equilibrium and kinetic studies of methyl orange and methyl violet adsorption on activated carbon derived from Phragmites australis, Desalination 252 (2010) 149–156. https://doi.org/10.1016/j.desal.2009.10.010.

[7] B. Shi, G. Li, D. Wang, C. Feng, H. Tang, Removal of direct dyes by coagulation: The performance of preformed polymeric aluminum species, J. Hazard. Mater. 143 (2007) 567–574. https://doi.org/10.1016/j.jhazmat.2006.09.076.

[8] T.A. Saleh, Advanced nanomaterials for water engineering and hydraulics, IGI Global, 2017.

[9] H. Zhu, R. Jiang, Y. Fu, Y. Guan, J. Yao, L. Xiao, G. Zeng, Effective photocatalytic decolorization of methyl orange utilizing TiO 2/ZnO/chitosan nanocomposite films under simulated solar irradiation, Desalination 286 (2012) 41–48. https://doi.org/10.1016/j.desal.2011.10.036.

[10] J.L.Bredas, Mind the gap!, Mater Horizons, 2014.

[11] S.Y. Janbandhu, S. CT, S.R. Munishwar, J.R. Jayaramaiah, R.S. Gedam,

Borosilicate glasses containing CdS/ZnS QDs: A heterostructured composite with enhanced degradation of IC dye under visible-light, Chemosphere 286 (2022) 131672. https://doi.org/10.1016/j.chemosphere.2021.131672.

[12] J.E. Shelby, Introduction to Glass Science and Technology, 2nd ed., The Royal Society of Chemistry, 2005.

[13] A. Sabir, T.A. Sherazi, Q. Xu, Porous polymer supported Ag-TiO2 as green photocatalyst for degradation of methyl orange, Surfaces and Interfaces 26 (2021) 101318. https://doi.org/10.1016/j.surfin.2021.101318.

[14] O. Örnek, Z.A. Kösemen, S. Öztürk, B. Canımkubey, Ş. Fındık, M. Erkovan, A. Kösemen, Performance enhancement of inverted type organic solar cells by using Eu doped TiO2 thin film, Surfaces and Interfaces 9 (2017) 64–69. https://doi.org/10.1016/j.surfin.2017.08.003.

[15] Y. Zhu, Y. Wang, Z. Chen, L. Qin, L. Yang, L. Zhu, P. Tang, T. Gao, Y. Huang, Z. Sha, G. Tang, Visible light induced photocatalysis on CdS quantum dots decorated TiO2 nanotube arrays, Appl. Catal. A Gen. 498 (2015) 159–166. https://doi.org/10.1016/j.apcata.2015.03.035.

[16] P.P. Pawar, S.R. Munishwar, R.S. Gedam, Eu2O3 doped bright orange-red luminescent lithium alumino-borate glasses for solid state lighting, J. Lumin. 200 (2018) 216–224. https://doi.org/10.1016/j.jlumin.2018.04.026.

[17] S.R. Munishwar, P.P. Pawar, S. Ughade, R.S. Gedam, Size dependent effect of electron-hole recombination of CdS quantum dots on emission of Dy3+ ions in boro-silicate glasses through energy transfer, J. Alloys Compd. 725 (2017) 115–122. https://doi.org/10.1016/j.jallcom.2017.07.146.

[18] A.S. Gadge, S.Y. Janbandhu, R.S. Gedam, Exploring the photocatalytic and antibacterial activity of Ce-doped TiO2 nanoparticles with remarkable self-cleaning superhydrophilic surface for outdoor application, Ceram. Int. 51 (2024) 602–611. https://doi.org/10.1016/j.ceramint.2024.11.038.

[19] C.Y. Huang, R.T. Guo, W.G. Pan, J.Y. Tang, W.G. Zhou, H. Qin, X.Y. Liu, P.Y. Jia, Eu-doped TiO2 nanoparticles with enhanced activity for CO2 phpotcatalytic reduction, J. CO2 Util. 26 (2018) 487–495. https://doi.org/10.1016/j.jcou.2018.06.004.

[20] A.S. Gadge, S.Y. Janbandhu, G.K. Sukhadeve, R. Kumar, C.D. Gajbhiye, R.S. Gedam, TiO 2 Nanoparticles for Methylene Blue Dye Degradation: Effect of

Calcination Temperature , ECS J. Solid State Sci. Technol. 12 (2023) 086004. https://doi.org/10.1149/2162-8777/acf06f.

[21] U. shukla and B.G. sharma sharma, ravi, D.P. Bisen, X-ray diffraction: a powerful method of characterisation, Recent Sci. Technol. (2012). https://doi.org/pp,77-79.

[22] A.A.B.E. gabriel and H.Y. Enien, X- ray diffraction: Instrumentation and application, critical reviews in analytical chemistry, 2015. https://doi.org/10.1080/10408347.

[23] M. Subhadra, P. Kistaiah, Infrared and Raman spectroscopic studies of alkali bismuth borate glasses: Evidence of mixed alkali effect, Vib. Spectrosc. 62 (2012) 23–27. https://doi.org/10.1016/j.vibspec.2012.07.001.

[24] B.C. Smith, Fundamentals of Fourier Transform Infrared Spectroscopy., CRC Press, 2011.

[25] J.A. Griffiths, P. R., & de Haseth, Fourier Transform Infrared Spectrometry., Wiley, 2007.

[26] and P.A.T. Rochow, Theodore G., Introduction to microscopy, Springer science and business media, 1994.

[27] Z. Ning, X. Gong, R. Comin, G. Walters, F. Fan, O. Voznyy, E. Yassitepe, A. Buin, S. Hoogland, E.H. Sargent, Quantum-dot-in-perovskite solids, Nature 523 (2015) 324–328. https://doi.org/10.1038/nature14563.

[28] H.H. Perkampus, UV-Vis Spectroscopy and its application, Springer science and business media, 2013.

[29] L.A. Kolahalam, I. V. Kasi Viswanath, B.S. Diwakar, B. Govindh, V. Reddy, Y.L.N. Murthy, Review on nanomaterials: Synthesis and applications, Mater. Today Proc. 18 (2019) 2182–2190. https://doi.org/10.1016/j.matpr.2019.07.371.

[30] A. Gacem, ―Plasmon Inspired 2D Carbon Nitrides: Structural, Optical and Surface Characteristics for Improved Biomedical Applications, vol. 2, 2022. https://doi.org/10.3390/cryst12091213.

[31] G.D. Gilliland, Photoluminescence spectroscopy of crystalline semiconductors, 1997. https://doi.org/10.1016/s0927-796x(97)80003-4.

[32] S.Y. Janbandhu, U. Patra, G.K. Sukhadeve, R. Kumar, R.S. Gedam, Photocatalytic performance of glasses embedded with Ag-TiO2 quantum dots on photodegradation of indigo carmine and eosin Y dyes in sunlight, Inorg. Chem. Commun. 148 (2023) 110317. https://doi.org/10.1016/j.inoche.2022.110317.

[33] M.M. Viana, V.F. Soares, N.D.S. Mohallem, Synthesis and characterization of TiO2 nanoparticles, Ceram. Int. 36 (2010) 2047–2053. https://doi.org/10.1016/j.ceramint.2010.04.006.

[34] M.S.P. Francisco, V.R. Mastelaro, P.A.P. Nascente, A.O. Florentino, Activity and characterization by XPS, HR-TEM, Raman spectroscopy, and bet surface area of CuO/CeO2-TiO2 catalysts, J. Phys. Chem. B 105 (2001) 10515–10522. https://doi.org/10.1021/jp0109675.

[35] J.F. Xu, W. Ji, Z.X. Shen, W.S. Li, S.H. Tang, X.R. Ye, D.Z. Jia, X.Q. Xin, Raman spectra of CuO nanocrystals, J. Raman Spectrosc. 30 (1999) 413–415. https://doi.org/10.1002/(SICI)1097-4555(199905)30:5<413::AID-JRS387>3.0.CO;2-N.

[36] F. Boccuzzi, A. Chiorino, Preparation, Characterization, and Activity of Cu/TiO 2 Catalysts, I C 139 (1997) 129–139.

[37] S. Feng, M. Wang, Y. Zhou, P. Li, W. Tu, Z. Zou, Double-shelled plasmonic Ag-TiO2 hollow spheres toward visible light-active photocatalytic conversion of CO2 into solar fuel, APL Mater. 3 (2015). https://doi.org/10.1063/1.4930043.

[38] F. Bensouici, M. Bououdina, A.A. Dakhel, R. Tala-Ighil, M. Tounane, A. Iratni, T. Souier, S. Liu, W. Cai, Optical, structural and photocatalysis properties of Cu-doped TiO 2 thin films, Appl. Surf. Sci. 395 (2017) 110–116. https://doi.org/10.1016/j.apsusc.2016.07.034.

[39] N.L. Reddy, S. Emin, V.D. Kumari, S. Muthukonda Venkatakrishnan, CuO Quantum Dots Decorated TiO2 Nanocomposite Photocatalyst for Stable Hydrogen Generation, Ind. Eng. Chem. Res. 57 (2018) 568–577. https://doi.org/10.1021/acs.iecr.7b03785.

[40] Ö. Kerkez, I. Boz, Photo(electro)catalytic activity of cu2+-modified tio 2 nanorod array thin films under visible light irradiation, J. Phys. Chem. Solids 75 (2014) 611–618. https://doi.org/10.1016/j.jpcs.2013.12.019.

[41] S.Y. Janbandhu, S.R. Munishwar, G.K. Sukhadeve, R.S. Gedam, Effect of annealing time on optical properties of CdS QDs containing glasses and their application for degradation of methyl orange dye, Mater. Charact. 152 (2019) 230–238. https://doi.org/10.1016/j.matchar.2019.04.027.

[42] G.K. Sukhadeve, S.Y. Janbandhu, R. Kumar, D.H. Lataye, D.D. Ramteke, R.S. Gedam, Visible light assisted photocatalytic degradation of Indigo Carmine dye

and NO2 removal by Fe doped TiO2 nanoparticles, Ceram. Int. 48 (2022) 29121–29135. https://doi.org/10.1016/j.ceramint.2022.05.053.

[43] G. V. Khade, N.L. Gavade, M.B. Suwarnkar, M.J. Dhanavade, K.D. Sonawane, K.M. Garadkar, Enhanced photocatalytic activity of europium doped TiO2 under sunlight for the degradation of methyl orange, J. Mater. Sci. Mater. Electron. 28 (2017) 11002–11011. https://doi.org/10.1007/s10854-017-6883-9.

[44] G.B. Yitagesu, D.T. Leku, A.M. Seyume, G.A. Workneh, Biosynthesis of TiO2/CuO and Its Application for the Photocatalytic Removal of the Methylene Blue Dye, ACS Omega (2024). https://doi.org/10.1021/acsomega.4c03472.

[45] J. Xu, Y. Chen, Z. Dong, Y. Peng, Y. Situ, H. Huang, Strong effect of multi-electron oxygen reduction reaction on photocatalysis through the promotion of interfacial charge transfer, Appl. Catal. B Environ. 252 (2019) 41–46. https://doi.org/10.1016/j.apcatb.2019.03.075.

[46] X.J. Yang, S. Wang, H.M. Sun, X.B. Wang, J.S. Lian, Preparation and photocatalytic performance of Cu-doped TiO2 nanoparticles, Trans. Nonferrous Met. Soc. China (English Ed. 25 (2015) 504–509. https://doi.org/10.1016/S1003-6326(15)63631-7.

सर मोक्षगुंडम विश्वेश्वरय्या
("भारत रत्न" पुरस्कार से सम्मानित)